



OPEN

Deep learning-integrated MRI brain tumor analysis: feature extraction, segmentation, and Survival Prediction using Replicator and volumetric networks

Deependra Rastogi¹, Prashant Johri², Massimo Donelli^{3,4}, Seifedine Kadry^{5,6}, Arfat Ahmad Khan^{7✉}, Giuseppe Espa⁴, Paola Feraco⁸ & Jungeun Kim^{9✉}

The most prevalent form of malignant tumors that originate in the brain are known as gliomas. In order to diagnose, treat, and identify risk factors, it is crucial to have precise and resilient segmentation of the tumors, along with an estimation of the patients' overall survival rate. Therefore, we have introduced a deep learning approach that employs a combination of MRI scans to accurately segment brain tumors and predict survival in patients with gliomas. To ensure strong and reliable tumor segmentation, we employ 2D volumetric convolution neural network architectures that utilize a majority rule. This method helps to significantly decrease model bias and improve performance. Additionally, in order to predict survival rates, we extract radiomic features from the tumor regions that have been segmented, and then use a Deep Learning Inspired 3D replicator neural network to identify the most effective features. The model presented in this study was successful in segmenting brain tumors and predicting the outcome of enhancing tumor and real enhancing tumor. The model was evaluated using the BRATS2020 benchmarks dataset, and the obtained results are quite satisfactory and promising.

Keywords Brain tumor, Magnetic resonance imaging, Feature extraction, Segmentation, Survival days prediction, Deep learning, 3D replicator neural network, 2D volumetric Convolutional Network

MRI plays a crucial role in clinical imaging as it provides reliable and measurable information for diagnosis. It is used for various purposes such as imaging the musculoskeletal system, cardiovascular system, and particularly the central nervous system and neurological subsystems. MRI has significant advantages over conventional medical imaging methods^{15,44}. However, the interpretation of MRI can be affected by changes in intensity caused by B1 and B0 field nonuniformity^{12,56}. This can result in an uneven appearance of tissues, which can mislead image analysis algorithms and make it difficult for recognition models to detect abnormal areas.

Brain tumours are uncommon conditions that arise from growths of malignant cells that can originate anywhere in the brain⁴⁵. Tumours can be classified as malignant or benign based on the structure and presence of active cells. Malignant tumours have an irregular form and active cells, whereas benign tumours have a constant structure and no active cells²⁴. Glioblastomas and astrocytomas are high-grade tumours that are categorised as malignant, whereas meningiomas and gliomas are low-grade tumours that are benign.

The American Brain Tumour Society and the World Health Organisation⁷ have developed a grading system that goes from grade I to grade IV for the categorisation of benign and malignant tumours. Grades I and II gliomas are benign, whereas grades III and IV are regarded as malignant. While grade III and IV gliomas grow

¹School of Computer Science and Engineering, IILM University, Greater Noida, Noida 201306, UP, India. ²SCSE, Galgotias University, Greater Noida, Noida 203201, UP, India. ³Department of Civil, Environmental, Mechanical Engineering University of Trento, Trento 38100, Italy. ⁴Radiomics Laboratory, Department of Economy and Management, University of Trento, Trento 38100, Italy. ⁵Department of Computer Science and Mathematics, Lebanese American University, Beirut, Lebanon. ⁶Noroff University College, Kristiansand 4612, Norway.

⁷Department of Engineering, Simpson University, California 96003, USA. ⁸Neuroradiology Unit, Santa Chiara Hospital, Azienda provinciale per i servizi sanitari, Trento 38100, Italy. ⁹Department of Computer Engineering, Inha University, Incheon, Republic of Korea. ✉email: arfat_ahmad_khan@yahoo.com; jekim@inha.ac.kr

quickly, low-grade tumours, such as grade I and II gliomas, grow more slowly⁵³. A low-grade brain tumour has the potential to progress to a malignant, high-grade brain tumour if treatment is not received. CNS neoplasms are classified into many categories in the WHO 5th edition⁴⁰, including meningiomas, embryonal tumours, pineal tumours, and CNS metastases.

The 5th edition of the blue book, which is an update from the 4th edition (Fig. 1) released in 2016, has undergone major changes in the classification of gliomas, glioneuronal and neuronal tumors, and embryonal tumors. The new edition has introduced 14 newly identified gliomas and glioneuronal tumors. Furthermore, diffuse gliomas are now classified by the WHO as either adult or paediatric-type neoplasms⁴⁰.

Low-grade benign tumors, such as grade I and II gliomas, can be treated by complete surgical removal. On the other hand, malignant brain tumors of grade III and IV can be cured through a combination of radiation, chemotherapy, or both. Malignant gliomas, including anaplastic astrocytoma's, can be found in both grade III and grade IV tumors⁴³. Anaplastic astrocytoma is a mid-grade tumor with an unusual or unpredictable growth pattern and a higher growth rate than low-grade tumors. Glioblastoma, the most severe type of astrocytoma, is the highest-grade glioma. Unlike other tumor grades, glioblastoma is characterized by the presence of dead cells (necrosis) around the tumor and the rapid growth of blood vessels¹⁰.

Medical image segmentation is necessary to isolate contaminated tumour tissues. Segmentation involves dividing an image into distinct parts or blocks based on shared features like colour, texture, contrast, brightness, boundaries, and greyscale levels. MR images or other imaging techniques are utilized for segmenting brain tumors into solid tumors, which may include cerebrospinal fluid, grey matter (GM), and white matter (WM), as well as separating them from central nervous system tissues and edema (CSF)¹⁰.

This research or medical imaging study that focuses on the analysis of brain tumor data obtained from MRI (Magnetic Resonance Imaging) scans. The objective of this study is to extract meaningful features from brain tumor images, segment the tumor regions, and predict the survival days of patients using a combination of deep learning techniques. The study employs a particular set of techniques to achieve its objectives, specifically a 2D volumetric convolutional network and a 3D replicator neural network influenced by deep learning. An MRI is a non-invasive imaging method that offers comprehensive details on the interior anatomy of the brain, including tumours. Feature extraction is the process of taking pertinent features out of the pictures of brain tumours. Among the traits that can be used to distinguish tumour areas from healthy brain tissue include form, texture, intensity, and other distinguishing qualities. Tumour locations within the MRI images are identified and delineated by a procedure known as segmentation. This process is essential for separating the tumour from the surrounding healthy tissue and isolating the affected region. In this study, another neural network architecture

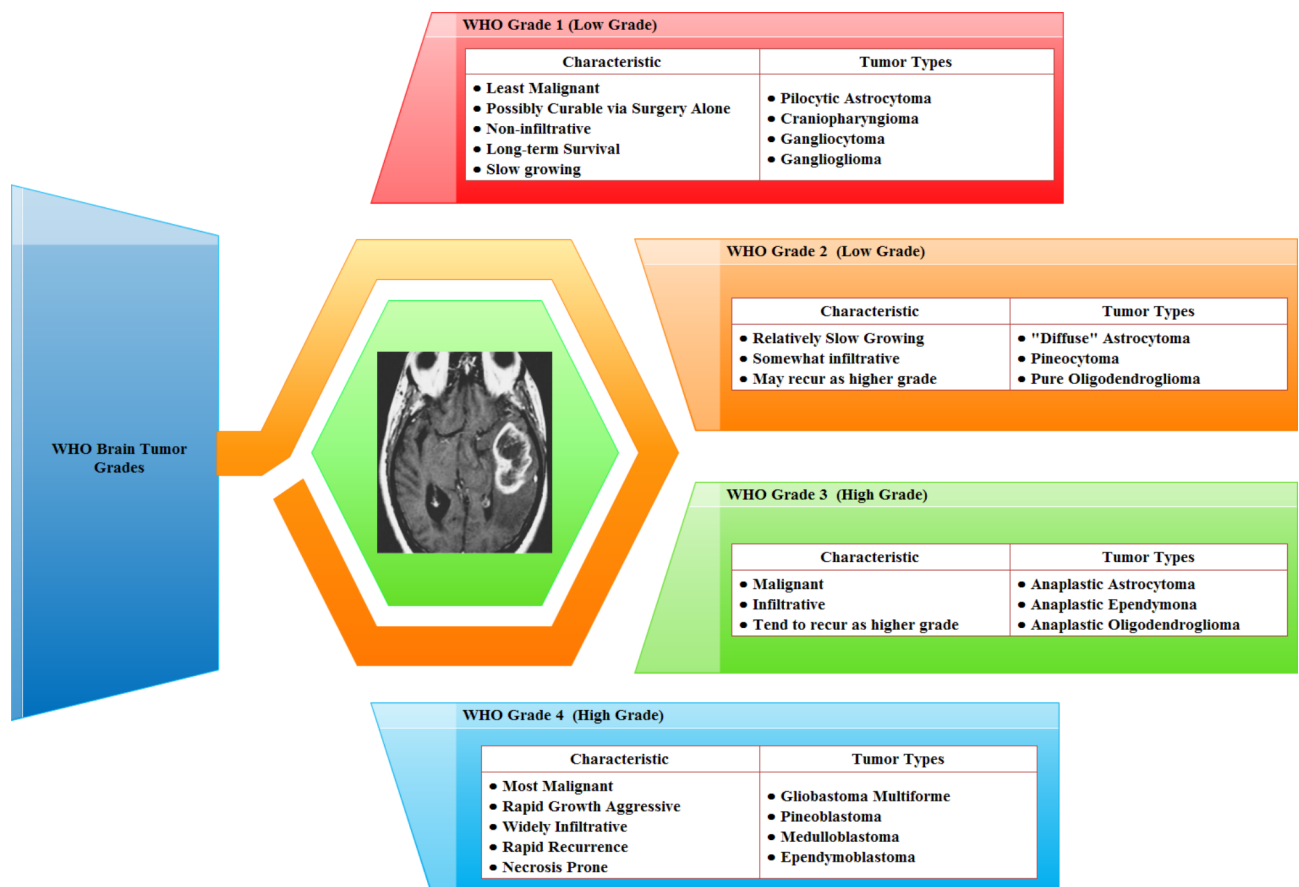


Fig. 1. WHO 4th Edition Glioma's Grading³⁷.

used is the 2D Volumetric Convolutional Network. To process the divided tumour zones and forecast survival days, it probably makes use of 2D convolutional layers. The replicator neural network can effectively extract meaningful representations from the tumour data by utilising deep learning techniques. This study analyses brain tumour data from MRI images using cutting-edge deep learning algorithms. The study attempts to forecast patients' survival days by using predictive models, segmenting tumour locations, and extracting significant characteristics, which will provide important information for clinical decision-making.

This study employs a variety of magnetic resonance imaging (MRI) patterns, including fluid-attenuated inversion recovery-weighted MRI, proton density weighted MRI, T2-weighted MRI, and T1-weighted MRI, to identify brain tumours. Effective treatment for brain tumours depends on early detection. Radiological study is required when there is a clinical suspicion of a brain tumour in order to pinpoint the exact location, extent, and influence on adjacent regions. Based on this information, the most suitable treatment, whether it be surgery, radiation therapy, or chemotherapy, can be determined. Early detection of a tumour can significantly increase the chances of patient survival. Figure 2 illustrates the visualization for multimodal scan of brain MRI.

The significant contribution introduced by the research study under consideration can be listed as follows:

1. The paper likely contributes to the field of brain tumor analysis by proposing a methodology that involves extracting meaningful features with the help from Replicator Neural Network from MRI images of the brain. This is a critical step in diagnosing and understanding brain tumors.
2. Volumetric Convolution Networks, which process 3D data, are particularly relevant for medical image analysis like MRI scans. This paper introduces ways to utilize such networks to segment brain tumors accurately and efficiently.
3. Predicting survival days based on medical images and patient data is a challenging task with significant clinical implications. The paper might contribute by proposing a deep learning-based model that predicts survival outcomes, which could assist medical professionals in treatment planning and patient management.

The rest of this article is organized Fig. 3 as follows. Section [Related work](#) provides a review of relevant previous research. In Sect. [Materials and methodology adapted](#), we outline the materials and methodology that we used in our study. Section [Measuring parameter and experimental results](#) is dedicated to presenting the measuring parameters and experimental results. Section [Discussion](#) includes a discussion of our findings and a comparison with existing models. Finally, in Sect. [Conclusion](#), we wrap up our work with concluding thoughts and suggestions for future improvements.

Related work

The research⁴² introduces a deep convolutional neural network (CNN) framework that utilizes several layers and variables to accurately and autonomously identify and separate brain cancer from MRI datasets. By using a skip connection with cardinality, the suggested model addresses the issue of gradient decay, lightens the computation complexity on the deep CNN architecture, and improves pixel quality. The F1-score, Jaccard Index, recall, DICE score, and other metrics are used to assess the model's performance in terms of accuracy. The UnetResNet-50

Multimodal Scans - Data | Manually-Segmented mask - Target

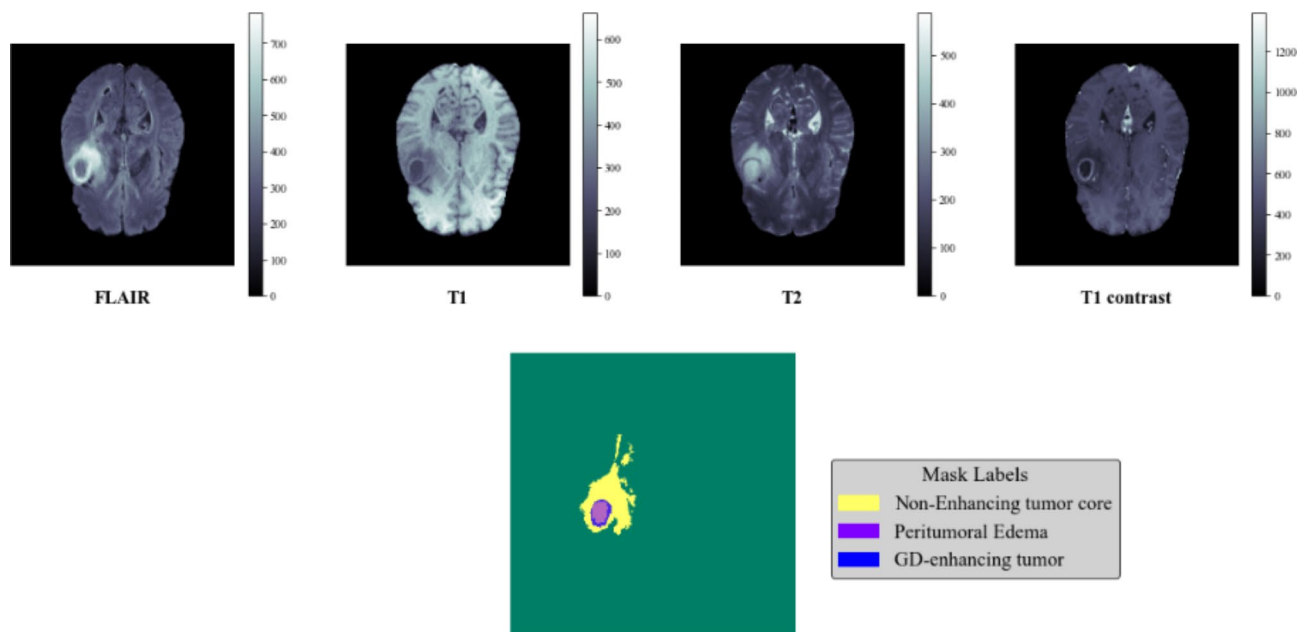


Fig. 2. Visualization for multimodal scan of brain MRI.

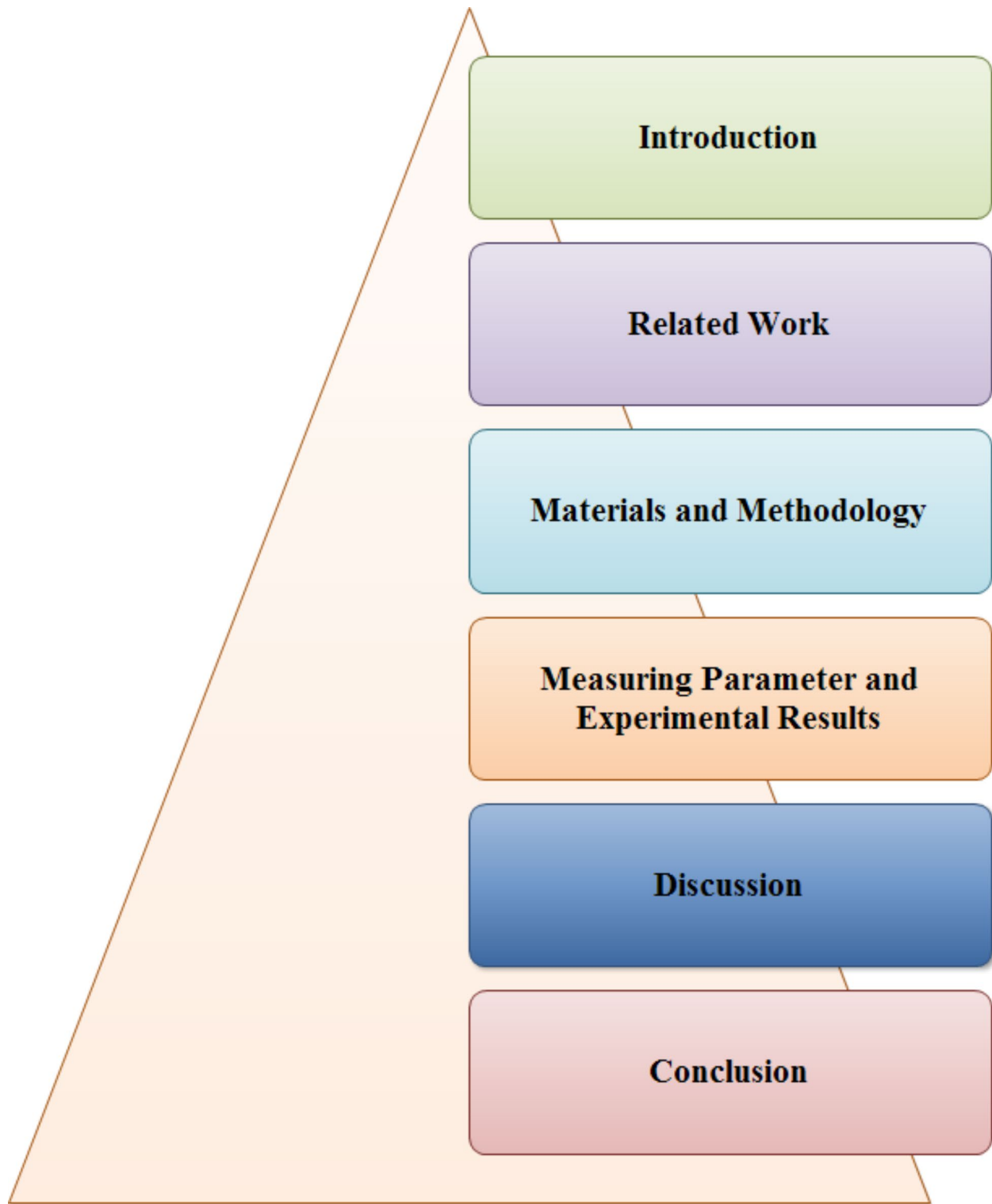


Fig. 3. Organization of the paper.

and Vanilla Unet models are contrasted with the UnetResNext-50 model as well as cutting-edge methods. The DICE score for the UnetResNext-50 model is 95.73, and it has a 99.7% accuracy rate.

A convolutional neural network (CNN) is employed in study¹¹ to classify brain tumours into five groups based on MRI data. Based on the input pictures, the proposed method identifies and learns deep properties using a convolutional autoencoder neural network (CANN). The deep aspects of each level are combined to generate new, stronger elements that enhance overall performance. The proposed technique has an impressive

accuracy rate of 99.3% when tested on the Cheng dataset, which classifies brain tumours into three categories: meningioma, glioma, and pituitary.

The goal of the research reported in the publication⁸ is to use deep learning to construct a model that can differentiate between input slices containing tumorous and healthy tissue. To address the inhomogeneities and field effects of the combined MR and input slices, a high-pass filter image is utilised. A median filter processing step is also applied to the fused slices to improve the quality of the output slices as well as to smooth and highlight the edges of the input slices. The authors then cluster the relevant pixels using a suitable threshold, and they use a 4-connected seed growth approach to group comparable pixels from the input slices based on intensity.

The article²⁰ suggests a technique for extracting brain tumor MRI images, including meningioma, glioma, and pituitary tumors. The method involves using transfer learning to distinguish image features from GoogLeNet encodings. The GoogLeNet encodings are then represented in a 2D feature space using a Siamese Neural Network (SNN). To train the SNN, a contrastive loss function is employed to teach it the distinct features of each image type. The lower-dimensional feature space is then used to compare query images to database images using the Euclidean metric. This strategy achieves excellent results in retrieving brain tumor MRI images.

Several techniques for feature extraction and categorisation of MR images are investigated in this work⁹. The authors have combined the benefits of the Discrete Wavelet Transform (DWT) and Bag-of-Words approaches to create a unique BoW method. Three datasets (DS-66, DS-160, and DS-255) containing 256×256 photos from Harvard Medical School are used to assess the system's effectiveness. The k-fold stratified Cross Validation (CV) approach is used in the validation step, yielding accuracy scores of 100%, 100%, and 99.61% for the DS-66, DS-160, and DS-255 datasets, respectively. Every MR image is computed in around 0.027 s on average.

This study⁵⁰ suggests a technique that uses texture characteristics and kernel sparse coding to distinguish brain tumours from FLAIR contrast-enhanced MRIs. After eliminating noise and enhancing contrast and intensity non-uniformity, a 3×3 patch surrounding the voxel is sparsely coded using statistical eigenvectors. Using kernel dictionary learning, non-linear characteristics are retrieved to produce two adaptive dictionaries: one for healthy tissue and another for damaged tissue. After that, the voxels are identified using linear discrimination and coded using a kernel-clustering technique based on dictionary learning. Finally, the flood-fill process is used to improve the segmentation quality.

Neural networks are another technique that has been proposed in this field¹⁹ for the identification and classification of brain tumours. A neural network-based classifier with 83% potential accuracy can segment white matter, grey matter, cerebrospinal fluid, and tumour regions with good quality. Moreover, it can divide tumour, grey matter, and white matter areas. A different paper⁴⁶ presents a method for automatically detecting brain tumours using MR images. Combining the MRMR methodology with an SVM-based classifier and Fast Fourier Transform-based feature extraction improves the accuracy of this approach, which obtains a 98.9% classification rate.

According to studies²⁵, brain cancers may be distinguished in MR images by being divided into two parts: one having tumour cells and the other holding normal cells. For brain tumour segmentation, a strategy combining seed region growth, Jaccard similarity coefficient algorithms, and FCM is suggested in⁵⁸. At noise levels ranging from 3 to 9%, the method achieves an average segmentation score of 90%. A method for autonomously segmenting brain tissues from MR images utilising feature selection and discriminative clustering algorithms is described in³³. Another method proposed in²¹ divides brain MR images into tumour, white matter (WM), grey matter (GM), edema, and cerebrospinal fluid (CSF) with high efficiency using wavelets and neural networks. Studies^{23,51} have examined the use of wavelet transformations, texture features, and SVM algorithms among other methods to categorise dynamic contrast-enhanced MR images. When compared to first-order statistical features, the method described in⁵⁷ produces superior predictions and improved clinical variables such cancer stage and volume.

A strategy for categorising brain tumours utilising a mix of PCA, RBF kernel, and SVM algorithms is presented in the paper³⁵. This method identified a total error rate of 7.5%, produced high similarity indices and overlap fractions of 96.20% and 95%, respectively, and had a 94% accuracy rate in categorising tumour kinds. An ANN and texture-primitive features are used in another technique published in⁴⁷ to 100% accurately diagnose brain tumours from MR images. In¹⁸, a new approach with accuracy rates ranging from 83 to 95% that successfully distinguished between cerebrospinal fluid, white matter, and grey matter in brain MR images employed localised fuzzy clustering with spatial information based on the Jaccard similarity score. To address intensity inhomogeneities in picture segmentation⁵⁴, developed a method utilising an active contour model. Furthermore¹⁵, proposed an automated GMM-based feature extraction method for brain tumour detection in MR images. By using PCA and wavelet-based features, the GMM feature extraction approach performs well, yielding an accuracy rate of 94.11% for FLAIR weighted images and 97.05% for T1- and T2-weighted MR images.

Brain tumours may be precisely segmented and categorised using a technique described in³¹ that combines Artificial Neural Networks (ANN) and Modified Fuzzy C-Means Clustering (MFCM). The method is taking MR images of brain tumours and extracting shape, texture, and intensity data, which are then enhanced with the Hybrid Fruit Fly and Artificial Bee Colony (HFFABC) algorithm. In order to monitor the decoder layer's learning process and enhance the feature map creation, a different suggested approach³⁸ proposes designing the generator with an independent loss function for each layer. Attention gates in Res-UNet's generator selectively focus on pertinent data instead of letting everything pass via skip connections.

For the detection of brain cancers in MRI images, B-CNN¹⁶ combines Convolutional Neural Network with the Bat algorithm. This method first pre-processes the data to eliminate noise, and then extracts the characteristics of the MRI brain images using the 2-D Gabor filter. The Bat algorithm selects the most relevant characteristics to improve accuracy.

The main aim of the study discussed in⁴ is to enhance the accuracy of brain tumour segmentation. To achieve this, the author suggests a novel architecture called MIRAU-Net, which incorporates residual and inception

modules with attention gates into the existing U-Net model. Inception Residual paths are used to connect encoder and decoder feature maps to reduce the distance between them. The problem of class imbalance is also tackled using a combination of weight cross-entropy, GDL, and focused Tversky loss functions.

Another approach for brain cancer classification is presented in²⁹, which is called CWCSD-enabled Deep CNN. The proposed method involves noise elimination and fractional probabilistic fuzzy clustering to segment the tumor region. The segmented regions are subjected to feature extraction using various techniques such as wavelet transform, scattering transform, information theoretic measures, LDP, and EMP. The study introduces a novel technique called Significant LOOP, which modifies SLBP through LOOP. These features are then used to train a Deep CNN model using the suggested CWCSD method to classify between non-tumor, edema, tumor, and increased tumor categories.

In this research²², a Convolutional Neural Network (CNN) based method is presented to segment and classify brain tumours from magnetic resonance images. The proposed technique achieves specificity, sensitivity, high accuracy, F1-score and precision for brain tumour segmentation.

This study²⁵ is presented brain cancers segmentation in MRI images by utilizing a combination of the watershed method and threshold segmentation, followed by classifying brain tumours using various classifiers based on extracted features such as MSER, FAST, and Harlick, among others. The suggested approach includes multiple steps such as image pre-processing, image acquisition, feature extraction and image segmentation.

Based on the analysis of related research, the following limitations have been identified:

- Brain tumors can manifest a wide range of characteristics encompassing size, morphology, texture, and intensity. Coping with this diversity effectively in feature extraction and segmentation methods can pose challenges.
- Medical images, such as MRI scans, are susceptible to the presence of disturbances and artifacts, potentially impacting the precision of segmentation techniques. Moreover, brain tumor images are obtained using distinct MRI sequences (e.g., T1-weighted, T2-weighted, FLAIR), each yielding distinct information.
- The variability between different imaging modalities can complicate the segmentation process. In scenarios where tumors infiltrate healthy tissue, the delineation of tumor boundaries can be indistinct, rendering the accurate determination of boundaries problematic.
- The prediction of survival in brain tumor patients is an intricate endeavour accompanied by a multitude of difficulties. The accurate selection of pertinent features for survival prediction is of utmost importance. However, the identification of the most informative features from a heterogeneous amalgamation of clinical and imaging data can be intricate.

This paper employed a hybrid approach that uses a 3D Replicator Neural Network inspired by deep learning and 2D Volumetric Convolutional Network for feature extraction and segmentation to predict patient survival. Based on the findings, the researchers propose that their method is suitable for integration with clinical decision support systems to assist medical professionals or radiologists in initial screening and diagnosis.

Materials and methodology adapted Specification of image dataset

In this research, we evaluate the efficacy of our proposed method's feature extraction and segmentation using the BraTS2020 dataset, which consists of 368 brain MRI scans with labels, each having dimensions of 240*240 with 155 slices, and using one of the four imaging modalities, namely T1, T1C, T2, and FLAIR, as illustrated in Fig. 4. The experiment was performed on a machine equipped with an i7-6500U CPU running at 2.50 GHz, 16GB of RAM, and an NVIDIA GEFORCE GTX. Each imaging modality provides unique information for identifying brain tumours, such as healthy tissues can be identified on T1 images, tumour boundaries can be identified using T1C modality, edema regions can be discriminated from cerebrospinal fluid on FLAIR images, and T2 images are useful for determining edema tumour regions. All the imaging modalities are included in our proposed method and pre-processed before being utilized as input images for neural networks.

The visualization of MR images and their masks using unique image values, minimum and maximum values, and unique mask values is shown in Fig. 5. For the MR image dataset used in this study, one image had 1202 unique values, with minimum and maximum image values of 0 and 1. The number of unique mask values was given as (array ([0, 1], dtype=float32), array ([8727379, 200621])).

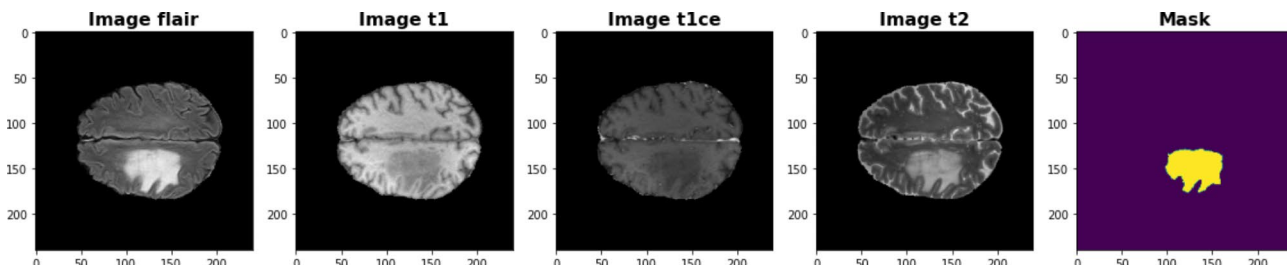


Fig. 4. Visualization of imaging modalities: T1C (contrast enhanced T1-weighted), T1 (T1-weighted), FLAIR (Fluid Attenuation Inversion Recovery), T2 (T2-weighted).

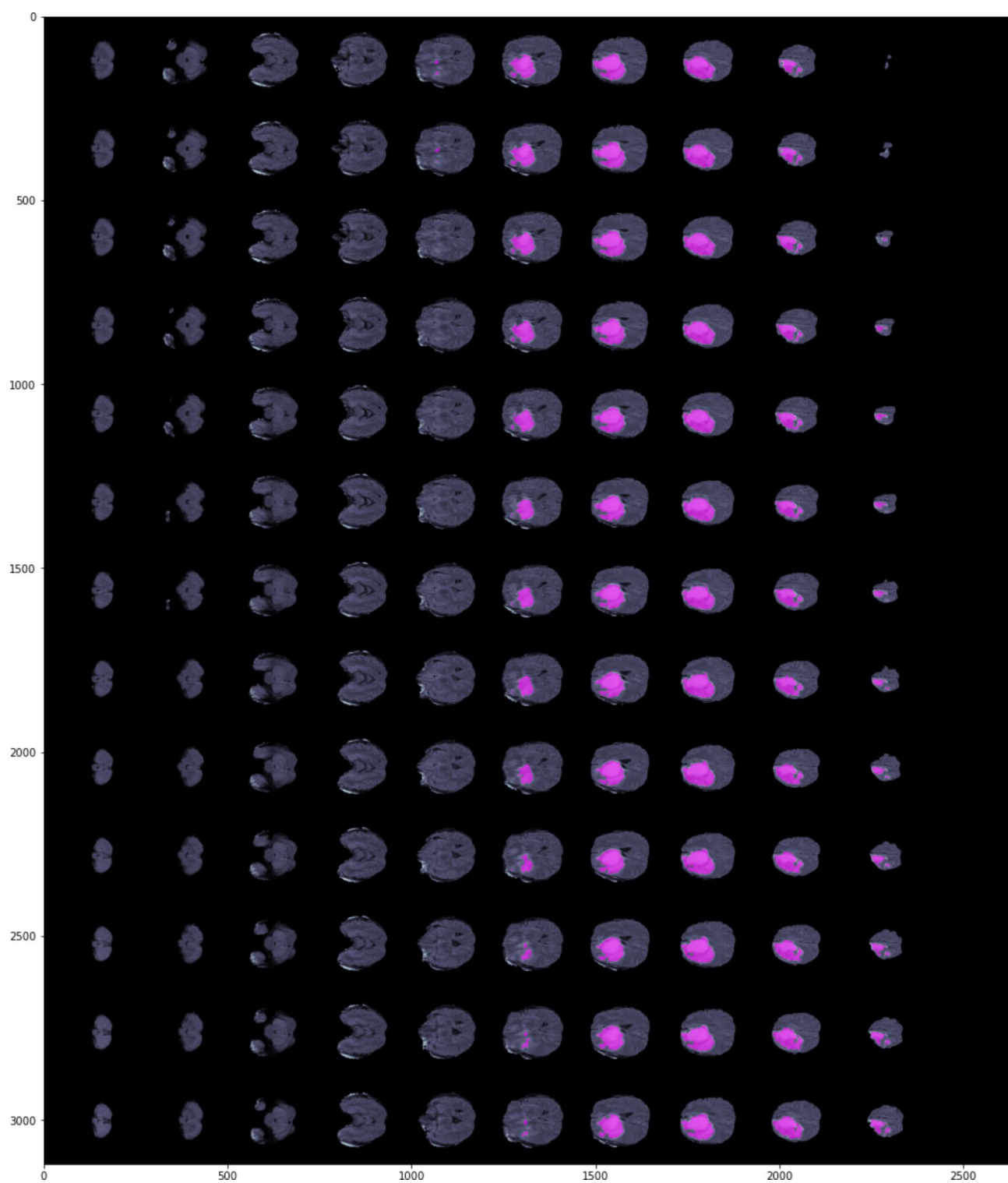


Fig. 5. Visualization of MR image and mask.

Preprocessing

The primary objective of pre-processing is to improve the clarity of MR images and convert them into a format that can be processed by humans or machine learning systems. Pre-processing also improves the visual quality of MR images by enhancing their signal-to-noise ratio, eliminating unwanted background elements and noise, smoothing the interior of regions, and maintaining their edges. The BRATS 2020 dataset contains 368 MR images in nii format. Due to memory limitations, this study used 150 MR images for the experiment, which were divided into three parts for training, testing, and validation (75%, 13%, and 12%). After resizing and inputting the images, the normalization step strengthens them and helps to address any potential issues

with feature extraction. The MinMax scaling technique was used to perform normalization. Normalization and standardization share the same basic concept of adjusting variables assessed at different scales to prevent bias in model fitting and learning functions. Therefore, feature-wise normalization, such as MinMax Scaling, is typically done before model fitting. In MinMax scaling, input variables are transformed to the range [0,1], with 0 and 1 being the maximum and minimum values for each feature/variable. The mathematical formulation for the min-max scaling is given by Eq. 1.

$$x_{scaled} = \frac{x - \min(x)}{\max(x) - \min(x)} \quad (1)$$

Deep learning models are known for their exceptional performance, but they do come with a few drawbacks. One of them is that they are susceptible to noise, which means that extensive pre-processing is required for every input visualize. To normalize MRI images with all characteristics, the pre-processing steps for segmentation and detection operations shown in Fig. 6 were followed.

- Step 1. To begin with, all the modalities and ground truth contain 3D volumes that have a dimension of $240 \times 240 \times 155$.
 - Step 2. Slicing these volumes results in 155 2D images with a measurement of 240×240 pixels.
 - Step 3. From each size, 90 portions ranging from 30 to 120 are selected.
 - Step 4. Finally, each MRI modality is reduced to a dimension of 192×192 by trimming the background noise.

Figure 7 represent the distribution graph for training, testing and validation.

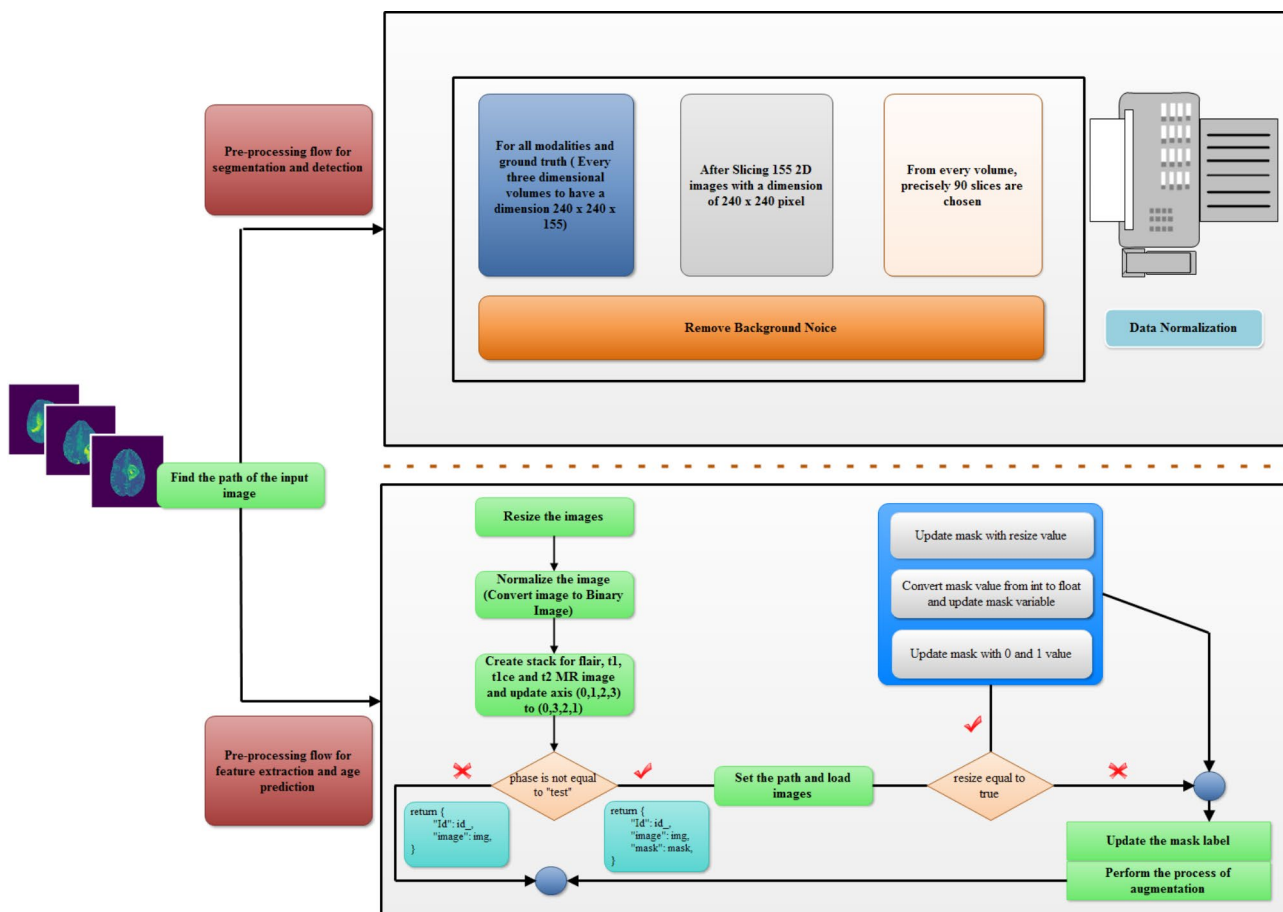


Fig. 6. Work flow for pre-processing.

BRATS 2020 MR Image Data Distribution

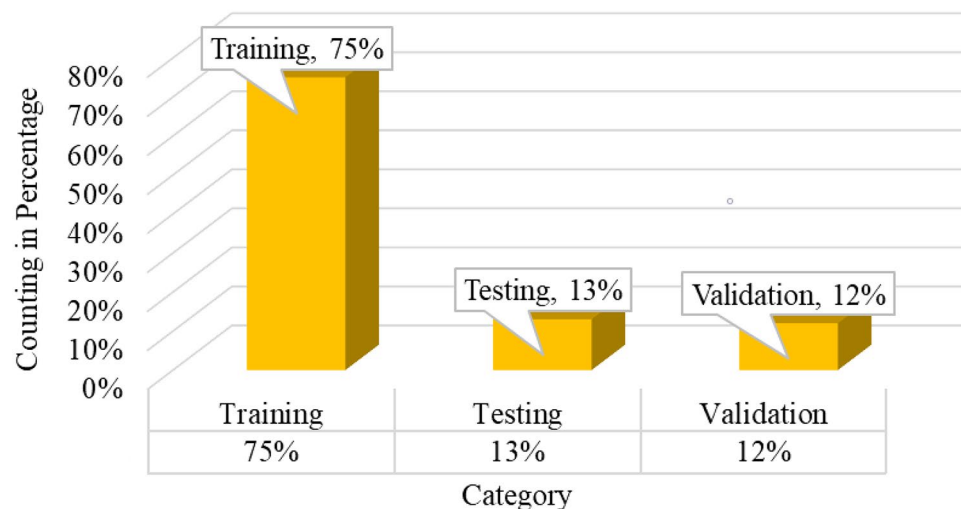


Fig. 7. Distribution graph for BRATS 2020 Dataset.

Pseudocode of class implementation for BRATS Dataset - Pre-processing for feature extraction process

Description: Here Dataset is a set of MR image that will used in the process of pre-processing

Initialization (instance of class, dataframe, phase, resize operation)

Description: Here the process of initialization will be acquired for pre-processing

- Set instance of class
- Set phase for dataset
- Set Augmentation variable to initialize with calling the function for given phase
- Set data_types for dataset images
- Set resize variable for images

Length (instance of class)

Description: Here to find the shape in dataframe

- Return the value of shape in dataframe

Fetch_Images(instance of the class , id for images)

Description: Here to find the location of BRATS images

- Set id for the location of BRATS images
- Set root_path to fatch the value
- Set variable for images to load all the modalities
- for data_type in class_instance.data_types
 - Set image_path as per given datatypes
 - Set variable img to load images from image_path
 - if class_instance.resize is true then
 - Update the img with new image size
 - Load value in img after the calling class_instance.normalize function with given img value as a pareameter
 - Append all the images
- Create a stack for the images
- Update the axis
- if class_instance.phase not equal to the passed value then
 - Set variable for the mask_path using the .seg value of MR image
 - Set variable mask for the loading of segmented value
 - if class_instance.resize is true then
 - Update mask with resize value
 - Convert mask value from int to float and update mask variable
 - Update mask with 0 and 1 value
 - Call the function to update the mask label
 - Perform the operation of augmentation
 - Set img and mask for augmented value of image and mask
 - Return value of id, image and mask
- Return id and image

Load_Images(class_instance, path of the file)

Description: This function to load all the images and convert into array form

- Set data variable to load value of file path
- Update data variable after converting into array
- Return data value

Normalize_data(class_instance, data as array form)

Description: This function dedicated to normalize the data as per min and max value of images

- Set datamin for minimum value of the data
- Return value of the expression $[(\text{data} - \text{datamin}) / (\text{max}(\text{data}) - \text{datamin})]$

Preprocess_label_mask(class_instance, mask as an array)

Description: Update mask value for the object of WT, TC and ET

- Update mask value for Whole Tumor with the value of 0 and 1
- Update mask value for Tumor Core with the value of 0 and 1
- Update mask value for Enhanced Tumor with the value of 0 and 1
- Create a stack for WT, TC and ET mask value
- Update the axis for mask value
- Return value of the mask

Network architecture and training approach for feature extraction, segmentation and detection

3D replicator neural network methodology

A replicator neural network is a type of feedforward neural network that reconstructs the output using the same input. It first reduces the input's dimension and then creates the output based on that representation. Replicator Neural Network is frequently used for unsupervised learning because they can help identify hidden relationships within data and present them in a more concise format. By transforming unsupervised learning issues into supervised learning algorithms, replicator neural network can be trained to identify patterns within data. The

input is passed through to the output, and an encoder network compresses the input into a smaller encoded form. Meanwhile, a decoder network decodes the encoding to reconstruct the input¹⁷.

The encoder layer generates a lower-dimensional version of the information, revealing complex and fascinating connections within the data. Figure 8 outlines the components of a replicator neural network.

- Encoder: The network component known as the encoder receives input and creates a lower-dimensional encoding which is known as the encoder.
- Bottleneck: The lower-dimensional hidden layer is the source of the encoding. The number of nodes present in the bottleneck layer is reduced, and it also determines how the input is encoded in terms of dimension.
- Decoder: The decoder receives the input and reconstructs it using the encoding.

Hyperparameters:

- Code Size: Signifies the number of intermediate layer nodes, where fewer nodes lead to more compression.
- Number of Layers: Depicts the number of layers that compose the network for the decoder and encoder.

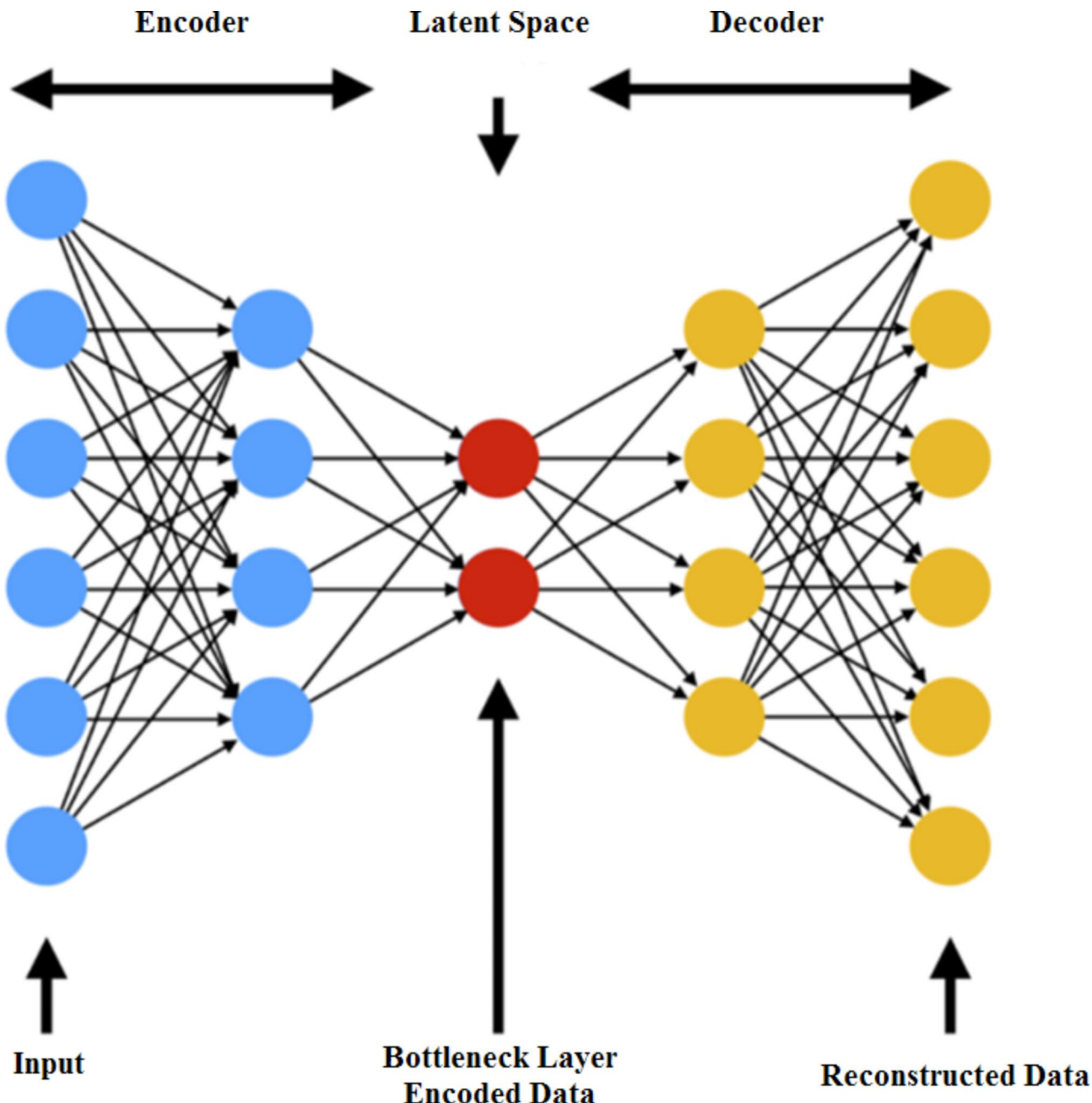


Fig. 8. Component of Replicator Neural Network with Latent Space³².

- Number of nodes per layer: The replicator neural network shown in the previous image is a stacked encoding network, meaning that the number of nodes per layer grows in the symmetric decoder while decreasing in the succeeding layers of the encoder.
- Loss Function: Cross entropy is commonly used if the input values are within the range [0, 1], otherwise Mean Squared Error should be used.

According to the following elements, replicator neural network is described: The spaces of decoded instructions (X) and encoded information (Z) are two sets. The majority of the time, X and Z are both Euclidean spaces, with $X = \mathbb{R}^m$ and $Z = \mathbb{R}^n$ for certain m and n .

There are two primary components of functions that have been parametrized: the encoder family $E_\emptyset : X \rightarrow Z$, parametrized by \emptyset ; and the decoder family $D_\theta : Z \rightarrow X$; parametrized by θ .

We often write $z = E_\emptyset$ for any value of $x \in X$ and refer to it by many names, including the code, latent variable, latent representation, latent vector, etc. On the other hand, we often write $x' = D_\theta(z)$ and correspond to this as the (decoded) message for any $z \in Z$.

Typically, multilayer perception is used to design both the encoder and the decoder. As an illustration, the one-layer MLP encoder E_\emptyset is

$$E_\emptyset(x) = \sigma(Wx + b) \quad (2)$$

The term “weight” refers to a matrix represented by W , “bias” refers to a vector indicated by b , and “activation function,” denoted by σ , is an element-wise function such as a sigmoid function or rectified linear unit (ReLU).

Training a replicator neural network

The training of proposed 3D replicator neural network consists of just a bundle of two factors on its own. Training needs an assignment in order to assess its quality. A benchmark probability distribution μ_{ref} over X and a “reconstruction efficiency” function $d : X \times X \rightarrow [0, \infty]$ are used to define a job, and $d(x, x')$ is a measurement of how far x' deviates from x .

These enable us to construct the replicator neural network’s loss function as

$$L(\theta, \emptyset) := \mathbf{E}_{x \sim \mu_{ref}} [d(x, D_\theta(E_\emptyset(x)))] \quad (3)$$

The presented replicator neural network for the assumed job (μ_{ref}, d) is then $\underset{\theta, \emptyset}{\operatorname{argmin}} L(\theta, \emptyset)$. Any mathematical optimization approach can be used to find the suggested replicator neural network.

The two primary components of replicator neural network are an encoder that converts a communication to a code and a decoder that extracts the information from the code. The recovery quality function d defines “near to perfect” as the performance that an ideal replicator neural network may achieve in terms of restoration.

Interpretation

Figure 9 illustrates how the 3D Replicator Neural Network for feature extraction interprets the model; the model is displayed after input has undergone pre-processing and normalisation, and the encoder has three convolutional layers, three pooling layers, and one linear layer.

Step 1 - Initialization for encoding representation is like that

$$\begin{aligned} \text{Convolutional Layer} &= \left\{ \begin{array}{l} conv1 \rightarrow conv3d(4, 16, 3) \\ conv2 \rightarrow conv3d(16, 32, 3) \\ conv3 \rightarrow conv3d(32, 96, 3) \end{array} \right. \\ \text{Pooling Layer} &= \left\{ \begin{array}{l} pool1 \rightarrow MaxPool3d(kernel_size = 2, stride = 2, return_indices = True) \\ pool2 \rightarrow MaxPool3d(kernel_size = 3, stride = 3, return_indices = True) \\ pool3 \rightarrow MaxPool3d(kernel_size = 2, stride = 2, return_indices = True) \end{array} \right. \end{aligned}$$

Step 2 - Initialization for decoding representation is like that

$$\begin{aligned} \text{Deconvolutional Layer} &= \left\{ \begin{array}{l} deconv1 \rightarrow ConvTranspose3d(96, 32, 2) \\ deconv2 \rightarrow ConvTranspose3d(32, 16, 3) \\ deconv3 \rightarrow ConvTranspose3d(16, 4, 3) \end{array} \right. \\ \text{Unpooling Layer} &= \left\{ \begin{array}{l} unpool1 \rightarrow MaxUnpool3d(kernel_size = 2, stride = 2) \\ unpool2 \rightarrow MaxUnpool3d(kernel_size = 3, stride = 3) \\ unpool3 \rightarrow MaxUnpool3d(kernel_size = 2, stride = 2) \end{array} \right. \end{aligned}$$

Step 3 – To perform the operation of Encoding the data frame:

$$conv1 \rightarrow pool1 \rightarrow conv2 \rightarrow pool2 \rightarrow conv3 \rightarrow pool3 \rightarrow Encoding_linear$$

After the process of the above mention layers, the Replicator Neural Network 3D model returns the features that will be decoded by the next steps.

Step 4 – The layering structure for the decoding as per the return features using deconvolution and unpooling like that:

Replicator Neural Network

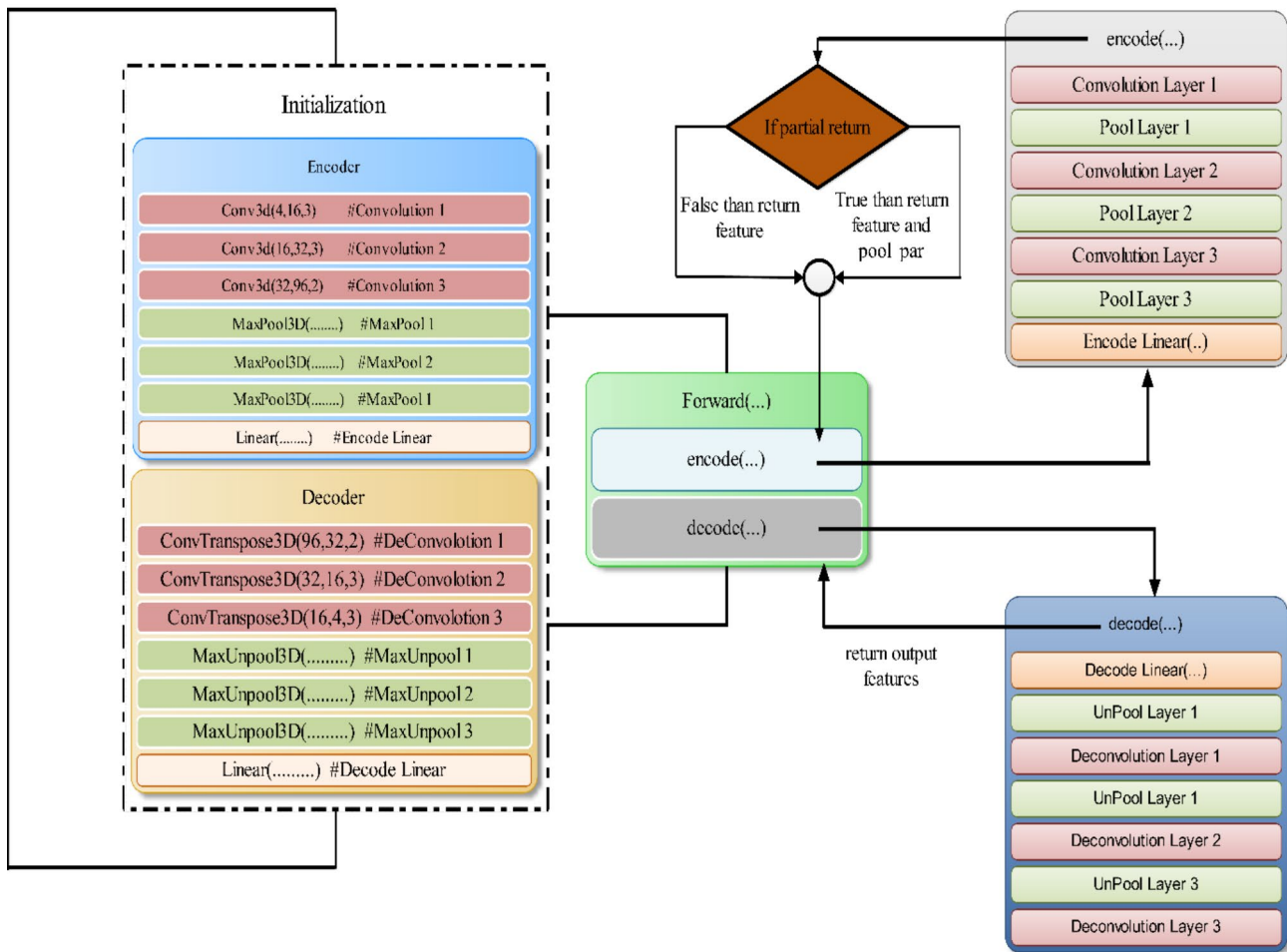


Fig. 9. 3D replicator neural network working flow.

Decoding_Linear → unpool1 → deconv1 → unpool2 → deconv2 → unpool3 → deconv3

2D Volumetric convolutional network methodology for segmentation and detection the tumor

The Fig. 10 illustration shows our conceptual convolutional neural network. Convolutional operations are utilized to extract features from the information, and after each stage, the data's resolution is reduced using an appropriate stride. The left side of the network compresses the signal, while the right side uncompresses it until it returns to its initial size³. Padding is suitably applied to convolutions throughout the network.

Left side of Network.

In this network, the left section handles different resolutions of the input data. The first three stages use convolutional layers to identify a residual function, which is trained using input from each phase, and then nonlinearly processed. This residual function ensures convergence, which is not possible in conventional learning networks without residual blocks. The convolutional operation uses a volumetric kernel with a voxel size of $5 \times 5 \times 5$.

The residual function plays a pivotal role in enhancing the convergence of deep neural networks, and its effectiveness can be better understood when compared to the compression path in a volumetric convolutional network. In such networks, the compression path reduces resolution using convolutions with a stride of 2 and $2 \times 2 \times 2$ voxel-wide kernels, halving the feature map size at each step, much like pooling layers. However, unlike pooling layers that use switches to map outputs back to inputs for backpropagation, the compression path doubles the number of feature channels at each step. This design choice ensures that, even as the spatial resolution decreases, the network retains sufficient information through an increased number of channels, facilitating the learning of complex features. The residual function, similar to this compression path, ensures the effective flow of information through the network by introducing shortcut connections. These connections allow the gradients to bypass certain layers, addressing the vanishing and exploding gradient problems, which are common in very deep networks. Just as the compression path increases the region of interest through down-sampling and introduces non-linearity via PReLU, the residual function simplifies the learning process by

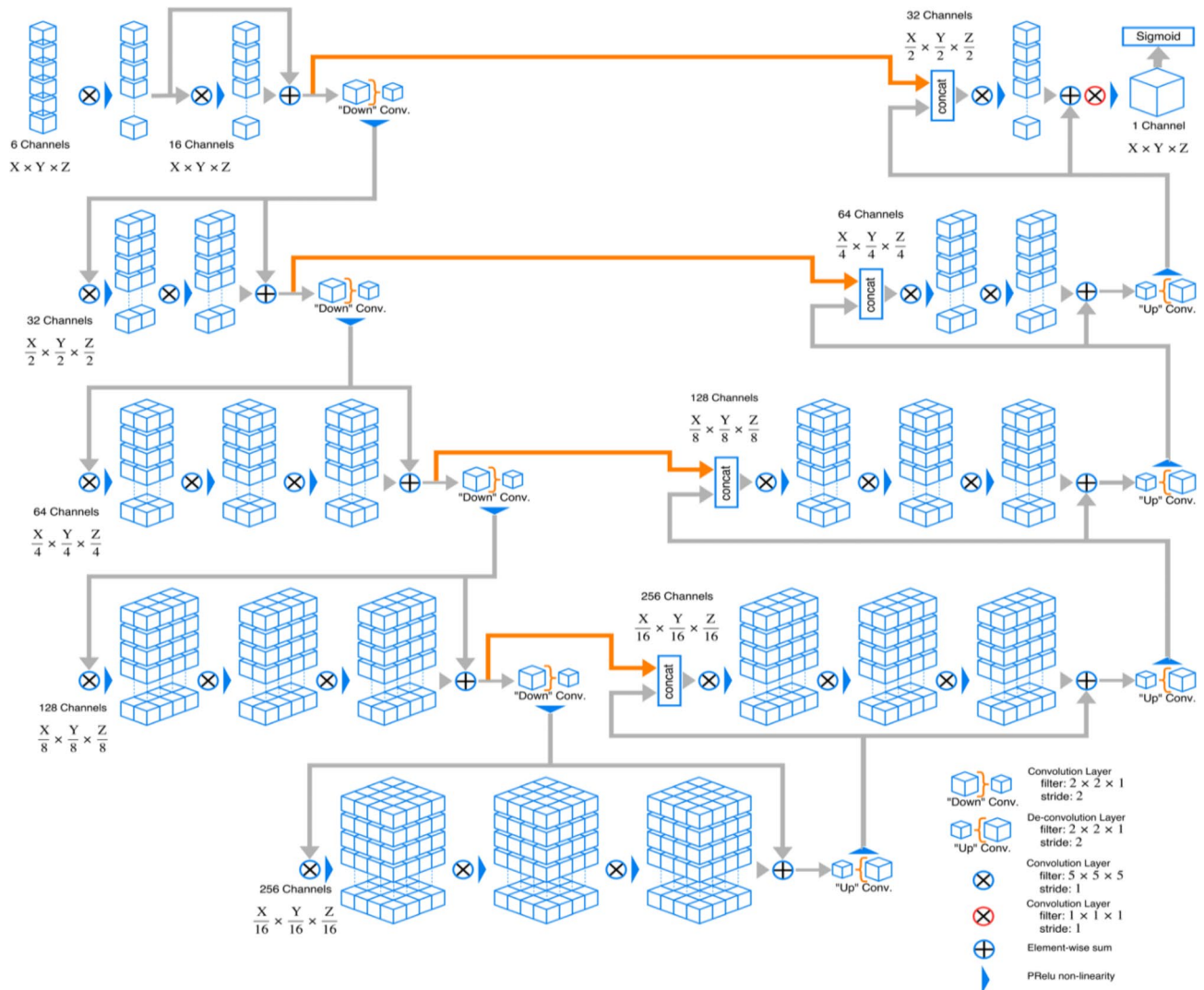


Fig. 10. Network Architecture for 2D Volumetric Convolutional Network³.

reformulating the task into learning residuals—differences between the input and the output—rather than full transformations. This simplification makes it easier for the network to optimize, much like how down-sampling in the compression path broadens the network’s focus. This mechanism also accelerates the convergence process, allowing the network to train more efficiently and effectively. Overall, the residual function facilitates better convergence by stabilizing gradients, simplifying learning, preventing degradation in deep networks, and optimizing the training process.

The Replicator Neural Network (RNN) architecture reduces memory usage through several key mechanisms. It efficiently encodes data into a lower-dimensional representation, significantly compressing the input data and reducing the size of intermediate activations. This encoding process requires fewer resources compared to the original high-dimensional data. The network also employs weight sharing across layers, which minimizes the total number of parameters that need to be stored. During training, this efficiency extends to reduced activation storage and more manageable backpropagation memory requirements.

Right Side of Network

By extracting features and increasing the geographic coverage of the lower resolution feature maps, the network tries to collect and synthesise the necessary data for producing a two-channel volumetric segmentation. Each level’s input size is increased using a deconvolution procedure, which is accompanied by one to three convolution operation that each have half as many 555 kernels as the layer before them. Similar to how the left half of the network is taught, so is the residual function. Two feature maps with the identical size as the source volume and 111 kernel strengths are produced by the last convolutional layer. The background and foreground areas are probabilistically divided into these two output feature maps using a soft-max voxel-wise method.

Horizontal Connection

The compression process of the CNN loses location information, as depicted on the left side. To resolve this issue, horizontal connections are incorporated to transmit elements from the early stages of the CNN’s left section to the right portion. This not only enhances the accuracy of the final contour prediction but also provides

precise position information to the right component. By incorporating these connections, the convergence time of the model is accelerated.

Step of Process Flow.

Step 1 Input Image for Data Pre-processing

- Each 3D volume of size $240 \times 240 \times 155$ is available for all modalities and ground truth.
- After converting into 2D pictures, there will be 155 images, each with dimensions of 240×240 pixels.
- Out of these 155 slices, only 90 slices ranging from 30 to 120 are selected from each volume.
- All MRI modalities are trimmed to 192×192 pixels to remove the background noise.

Step 2 Process of Data Normalization

Step 3 Splitting the normalized data 75% Training Data, 13% Testing Data, 12% Validation Data

Step 4 Apply 2D V-Net Model (Encoding and Decoding process on normalized Data)

Step 5 Applying Training model into Testing Data and Validation Data

- Find Dice coefficient
- Find Accuracy
- Find Loss Value

Step 6 Verify the result for prediction

The Parametric Rectified Linear Unit (PReLU) is used as the activation function in deep neural networks to address certain limitations of traditional activation functions, such as ReLU. PReLU introduces a small, learnable parameter for the negative slope of the activation function, allowing it to adaptively learn the best slope during training.

PReLU is defined as $f(x) = x$ for $x \geq 0$ and $f(x) = \alpha x$ for $x < 0$, where α is a learnable parameter. Unlike the standard ReLU, which sets all negative inputs to zero, PReLU allows a small gradient for negative values, thereby preventing the “dying ReLU” problem, where neurons can become inactive and stop learning if they output only zeros.

How PReLU Improves Model Performance:

- Avoiding Dead Neurons: By allowing a small gradient for negative values, PReLU prevents neurons from becoming inactive, ensuring that all neurons can contribute to learning throughout the training process. This helps maintain a more diverse set of features and prevents the network from becoming too sparse.
- Enhancing Learning: The adaptability of PReLU means that the network can learn the most effective slope for negative values during training. This flexibility can lead to better model performance as the network optimizes its activation function for the given task, improving its ability to capture complex patterns and relationships in the data.
- Improving Gradient Flow: The non-zero gradients for negative inputs help maintain a more stable and effective gradient flow during backpropagation. This stability aids in more consistent weight updates, which can accelerate convergence and improve overall training efficiency.
- Increased Model Capacity: PReLU’s ability to learn different slopes for positive and negative inputs effectively increases the network’s capacity to model complex functions. This enhanced flexibility allows the network to fit the training data more accurately and generalize better to unseen data.

Measuring parameter and experimental results

Feature extraction refers to the technique of obtaining more detailed data about an image, such as its texture, shape, contrast, and color. Texture analysis is a vital aspect of both machine learning systems and human visual perception. By selecting significant features, it can effectively enhance the accuracy of the diagnostic system. Textural observations and analysis can be beneficial in evaluating the different stages of tumours (tumour staging) and for diagnosis. The formula for some relevant statistical aspects and the results of the experiments are provided below.

Mean (M): The mean of the object is determined using, by multiplying the sum of all the pixel values in an object by the overall number of pixels present in the object.

$$M = \left(\frac{1}{m \times n} \right) \sum_{x=0}^{m-1} \sum_{y=0}^{n-1} f(x, y) \quad (4)$$

Experimental result of mean for the BRATS 2020 dataset with t1 weighted, t1ce weighted, t2 weighted and flair is shown in Fig. 11.

Skewness (Skn) Skewness is a metric for symmetry or lack thereof. The definition of the skewness of an arbitrary variable X, represented as $S_{kn}(X)$, is the determination of the image’s mean.

$$S_{kn}(X) = \left(\frac{1}{m \times n} \right) \frac{\sum (f(x, y) - M)^3}{SD^3} \quad (5)$$

Where SD is standard deviation and will be evaluated like that

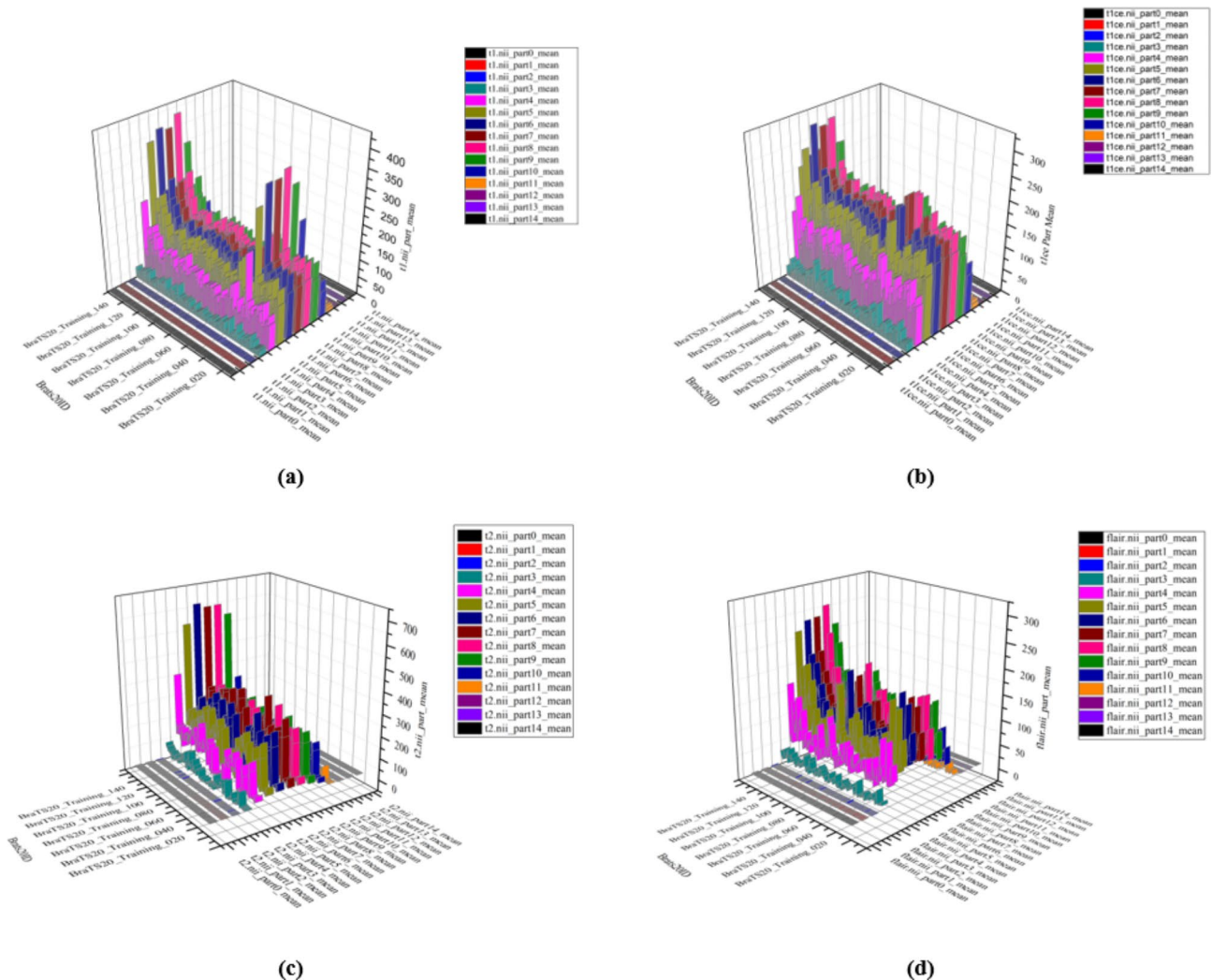


Fig. 11. Mean value experimental result for BRATS2020 MRI Dataset (a) t1 weighted values (b) t1ce weighted values (c) t2 weighted value (d) flair value.

$$SD(\sigma) = \sqrt{\left(\frac{1}{m \times n}\right) \sum_{x=0}^{m-1} \sum_{y=0}^{n-1} (f(x, y) - M)^2} \quad (6)$$

Experimental result of Skewness for the BRATS 2020 dataset with t1 weighted, t1ce weighted, t2 weighted and flair is shown in Fig. 12a.

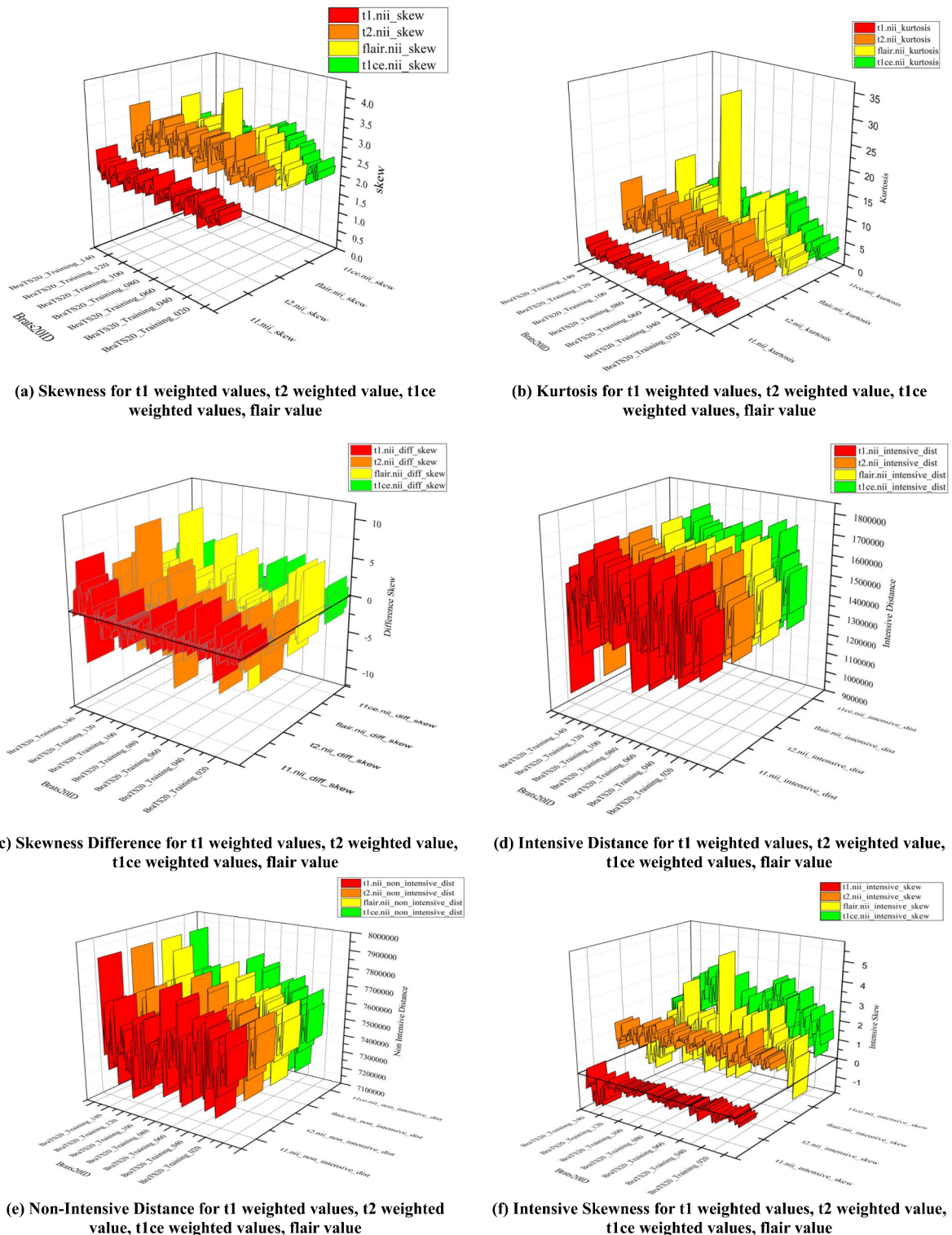
Kutosis (Krt) The Kurtosis parameter describes the probability distribution's form for a random variable. For the random identifier X, the Kurtosis is identified as $K_{rt}(X)$ and it is defined as.

$$K_{rt}(X) = \left(\frac{1}{m \times n}\right) \frac{\sum (f(x, y) - M)^4}{SD^4} \quad (7)$$

Experimental result of Kurtosis for the BRATS 2020 dataset with t1 weighted, t1ce weighted, t2 weighted and flair is shown in Fig. 12b.

Skewness Difference: Skewness Difference measures the disparity in asymmetry between two probability distributions or datasets. Skewness itself quantifies how a distribution deviates from symmetry around its mean: positive skewness indicates a longer tail on the right, while negative skewness suggests a longer tail on the left. By calculating the difference in skewness between two datasets, Skewness Difference provides insight into how their asymmetries compare. Figure 12c shows the experimental result of skewness differences for the BRATS 2020 dataset with t1 weighted, t1ce weighted, t2 weighted and flair.

Intensive Distance Intensive Distance is a concept used to measure the relative difference or similarity between data points or distributions while controlling for scale and size. Unlike traditional distance metrics, which often

**Fig. 12.** Features Value Graph for Skewness, Kurtosis, Intensive Differences.

consider absolute differences and may be influenced by the scale of data, Intensive Distance focuses on the inherent characteristics of the data by normalizing or adjusting for scale effects.

Figure 12d shows the experimental result of intensive distribution for the BRATS 2020 dataset with t1 weighted, t1ce weighted, t2 weighted and flair.

Non-intensive Distance Non-Intensive Distance is a concept used to measure the distance between data points or distributions without accounting for scale or variability adjustments. Unlike Intensive Distance, which normalizes for scale to ensure equitable comparisons, Non-Intensive Distance considers the raw differences between values or features directly. This approach does not adjust for the size or distribution of the data, making it sensitive to absolute values and scale. Figure 12e shows the experimental result of non-intensive distribution for the BRATS 2020 data set with t1 weighted, t1ce weighted, t2 weighted and flair.

Intensive skewness It is the measurement of skewness for intensive distribution data. Figure 12f shows the experimental result of intensive skewness for the BRATS 2020 dataset with t1 weighted, t1ce weighted, t2 weighted and flair.

Non-intensive Skewness It is the measurement of skewness for non-intensive distribution data. Figure 13a shows the experimental result of non-intensive skewness for the BRATS 2020 dataset with t1 weighted, t1ce weighted, t2 weighted and flair.

Data intensive skewness difference It evaluates the raw disparity in skewness between two datasets, reflecting the asymmetry differences without adjusting for scale or normalization. Figure 13b show the experimental result of Intensive Skewness Difference for the BRATS 2020 data set with t1 weighted, t1ce weighted, t2 weighted and flair.

Data non-intensive skewness difference It is the difference between data skewness and non-intensive skewness. Figure 13c shows the experimental result of data non-intensive skewness Difference for the BRATS 2020 data set with t1 weighted, t1ce weighted, t2 weighted and flair.

Latent feature A set of objects is embedded within a multidimensional in a latent space, often referred to as a latent feature space or embedding space (Fig. 13d). In the latent space, the items that are more similar to one another are placed closer to one another. Simply said, the latent space is a depiction of compressed data, where like data points are located near to one another. Latent space is helpful for discovering more straightforward visualisations for analysis as well as for learning data features.

To achieve better evaluation results on brain MR images, additional quality evaluation parameters to the one below mentioned are also required for segmentation.

Loss: A way to assess how effectively your programme models your dataset is via the Loss function. It is a mathematical function of the deep learning algorithm's parameters. In this proposed work, performance of a segmentation model is measured by cross entropy loss. A number between 0 and 1 represents the loss (or error), with 0 representing the ideal model. Generally speaking, the objective is to bring your model as close to 0 as you can. Using cross entropy, we can measure the error (or difference) between two probability distributions.

Cross-entropy, for instance, in the context of Binary Classification is provided by:

$$l = -(y \log(p) + (1 - y) \log(1 - p)) \quad (8)$$

Where, p is the predicted probability and y is the indicator.

Accuracy: A statistic used to assess the model's effectiveness across all classes is accuracy. When each class is given equal weight, it is very helpful. To determine accuracy, divide the total number of correct guesses by the total number of forecasts.

$$\text{Accuracy} = \frac{\text{True}_{\text{positive}} + \text{True}_{\text{negative}}}{\text{True}_{\text{positive}} + \text{True}_{\text{negative}} + \text{False}_{\text{positive}} + \text{False}_{\text{negative}}} \quad (9)$$

MeanIOU: Mean Intersection over Union (MeanIoU) calculates the proportion of the overlap between two bounding boxes to the union of the areas of the boxes. The prediction and the ground truth are contained within these bounding boxes. This metric can be used for any approach that predicts bounding boxes. Its mathematical formulation is:

$$J(A, B) = \frac{|A \cap B|}{|A \cup B|} \quad (10)$$

Dice Coefficient: The Dice similarity coefficient (DSC) was employed as a statistical validation metric to assess the repeatability of human segmentations and the spatial overlap accuracy of automated probabilistic fractional segmentation of MR images. This coefficient measures how similar two images are by dividing the total number of pixels in both images by the area of overlap between the two segmented images.

Precision: The model's accuracy is measured by the percentage of Positive samples that were correctly classified out of all samples that were classified as Positive, regardless of whether they were classified correctly or incorrectly. Precision, on the other hand, evaluates how effectively the model identifies a sample as positive.

$$\text{Precision} = \frac{\text{True}_{\text{positive}}}{\text{True}_{\text{positive}} + \text{False}_{\text{positive}}} \quad (11)$$

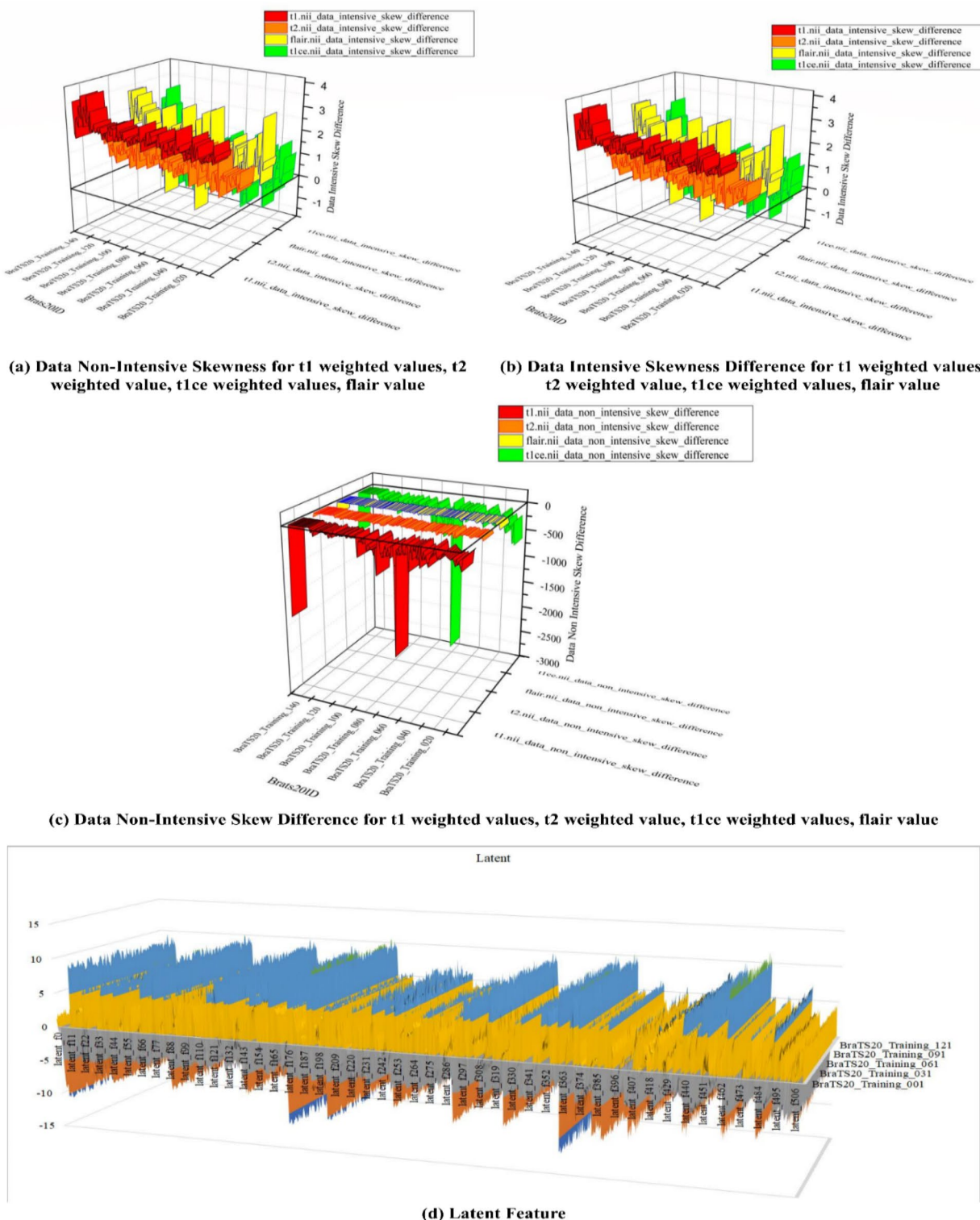


Fig. 13. The feature graph values for non-intensive skewness, intensive skewness, non-intensive skew differences, and latent features.

The denominator rises and the precision becomes low when the model makes many wrong Positive classifications or few correct Positive classifications. However, the precision is high when:

- Numerous accurate Positive classifications are made by the model (maximize True Positive).
- Less inaccurate Positive classifications are made by the model (minimize False Positive).

Sensitivity: The ability of a learning model to recognise good examples is referred to as its sensitivity. It is also known as the recall or the true positive rate (TPR). We can calculate the number of examples the model correctly identified using its sensitivity, which is why it is utilised to assess model performance. Few false negatives suggest that a model with high sensitivity is likely to be missing some of the positive examples. Sensitivity, in other words, assesses how well a model can recognise good samples. This is crucial because in order for our models to produce reliable predictions, they must be able to identify all of the positive cases.

$$Sensitivity = \frac{True_{positive}}{True_{positive} + False_{Negative}} \quad (12)$$

Specificity: The model's ability to correctly detect true negatives is referred to as specificity. This implies that some true negatives, which are classified as false positives, may be reported. This percentage can also be referred to as the True Negative Rate (TNR). When specificity (actual negative rate) and false positive rate are added together, they always sum up to one. While a model with low specificity could mistakenly classify many negative results as positive, one with high specificity can reliably identify the majority of negative outcomes.

$$Specificity = \frac{True_{negative}}{True_{negative} + False_{positive}} \quad (13)$$

	Sensitivity	Specificity	Dice Coefficient Necrotic	Dice Coefficient Edema	Dice Coefficient Enhancing
Train Result	0.995159	0.998398	0.873707	0.888389	0.886813
Validation Result	0.994502	0.998179	0.864612	0.875613	0.866567
Test Result	0.994176	0.998073	0.857214	0.877539	0.863696

Figure 14 shows the evaluation graphs with respect to each epoch. Figure 15 demonstrates how the model's forecast for segmenting a brain tumour is to produce an accurate picture of the tumor's position and size. Experiments using the proposed strategy have produced some illuminating findings. For the dataset we used, we have achieved a high degree of accuracy in detecting the presence of a tumour.

Survival prediction for brain tumors is a multifactorial and complex task that requires a comprehensive evaluation of various factors, including the type of tumor, location, stage, size, age, and overall health of the patient. There are various prognostic factors that can be used to estimate the survival rate of a patient with a brain tumor, such as the histological type, the degree of malignancy, the extent of resection, the presence of metastases, and the patient's age and overall health status. The graph Figs. 16 and 17 is representing the distribution of rounded ages of data as given in BRATS 2020.

Discussion

The study's results demonstrate that the application of a specific pre-processing technique and a carefully selected set of model parameters led to improved efficiency in both feature extraction and brain tumor segmentation during image segmentation tests.

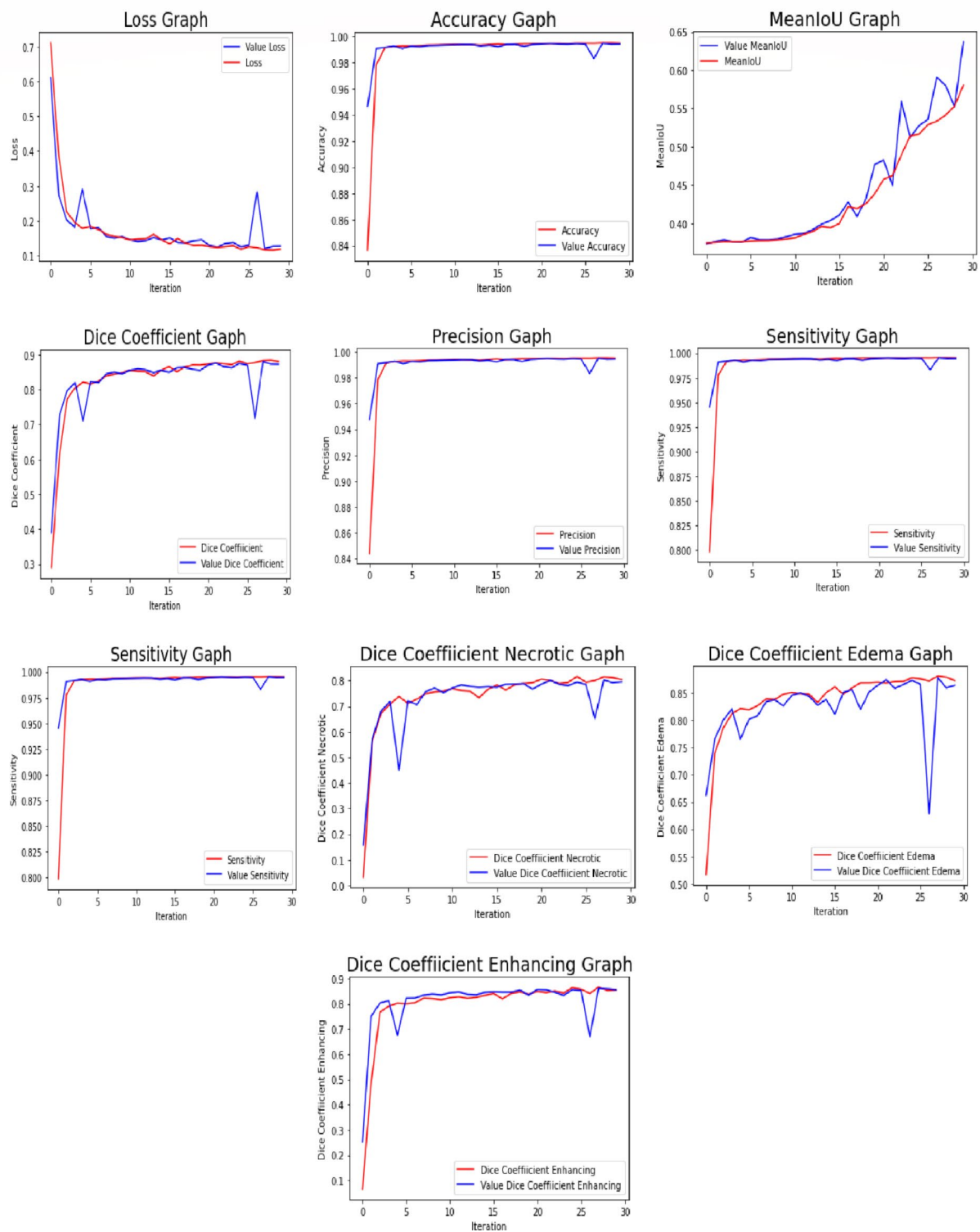
The experimental results of our proposed method offer some insightful information. With the dataset we utilised, we were successful in achieving high overall performance in detecting the presence of a tumour. Yet, it's crucial to keep the training data's big imbalances to a minimum. Tables 1 and 2 show the evaluation report and comparative analysis. By contrasting our outcomes with those of various cutting-edge techniques, we were able to show that our suggested strategy performed similarly to fully supervised alternatives.

Advantage of the adapted methodology.

- MRI Based Brain Tumor Feature Extraction, Segmentation and Survival Days Prediction using Deep Learning Inspired Replicator Neural Network and Volumetric Convolution Network.
- Utilizing deep learning techniques, such as Replicator Neural Networks and Volumetric Convolution Networks, can potentially lead to higher accuracy and robustness in feature extraction, segmentation, and survival prediction tasks.
- By incorporating survival prediction, the study could offer valuable insights for clinicians and researchers in understanding patient outcomes, treatment planning, and disease progression.

The approach of has several limitations:

- **Data Dependency:** The effectiveness of the model is heavily reliant on the quality and quantity of the available MRI data. Inconsistent data from different sources, such as varying image quality, scanner settings, and patient demographics, can impact the model's performance and generalization.
- **Computational Resource Requirements:** This approach involves complex neural network architectures that require significant computational resources, including high-performance GPUs and extensive memory. This can be a limitation for institutions with limited access to advanced hardware.
- **Training Time:** Given the complexity of the model, training can be time-consuming, particularly when working with large 3D MRI datasets. This can hinder rapid experimentation and model iteration, slowing down the development process.

**Fig. 14.** Evaluation Graph Epoch by Epoch.

- **Generalization Across Diverse Populations:** The model may struggle to generalize well across diverse patient populations due to differences in tumor characteristics, genetic factors, and treatment protocols. This limitation could reduce the model's accuracy when applied to new or underrepresented patient groups.
- **Interpretability Issues:** Deep learning models, including Replicator Neural Networks and Volumetric Convolution Networks, often operate as “black boxes,” making it difficult to understand the rationale behind their predictions. This lack of interpretability can be a barrier to clinical adoption, as clinicians need to trust and verify the model’s outputs.

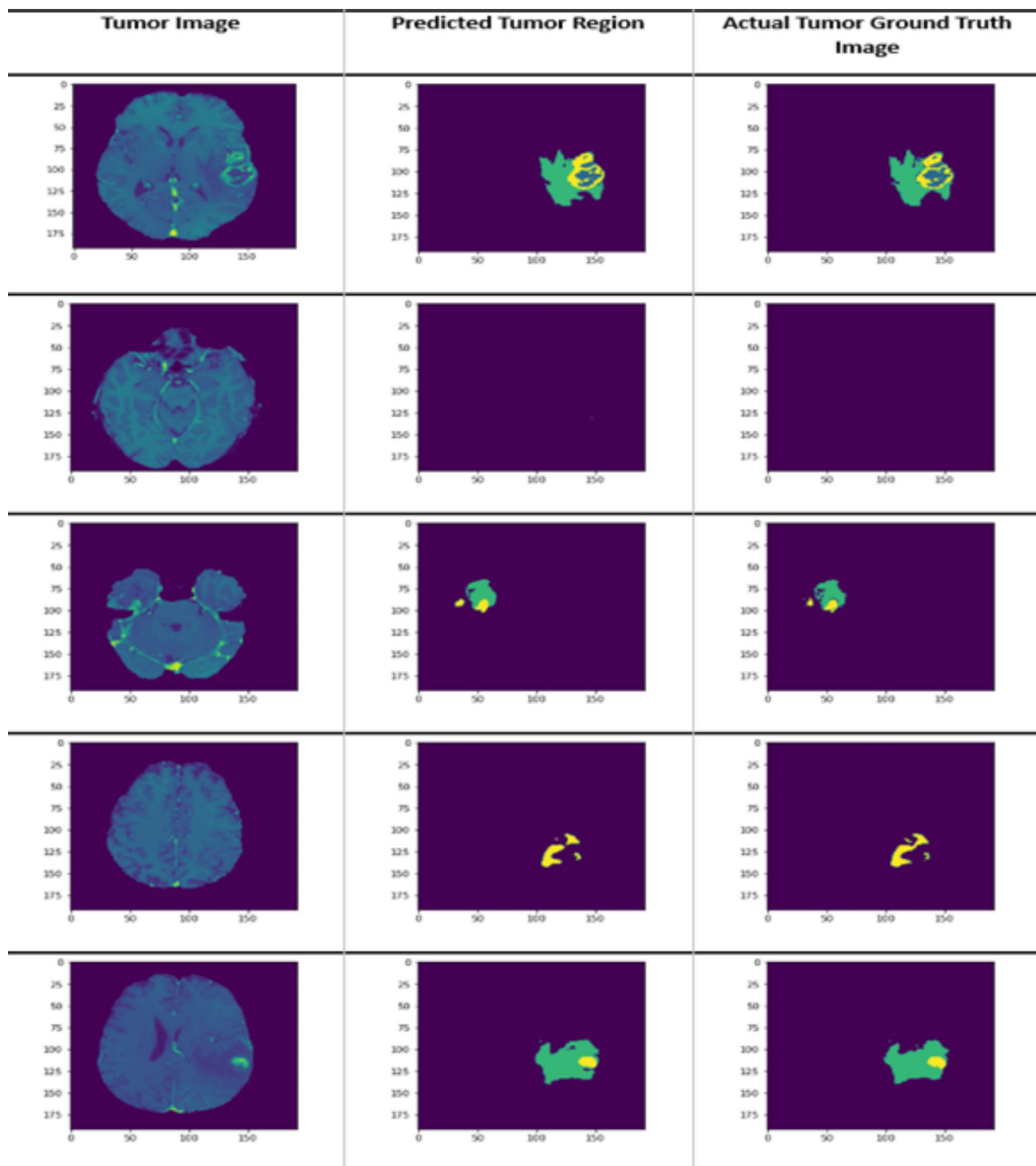


Fig. 15. The model's prediction after dividing the image into segments can be represented in three forms: (a) the original tumor image, (b) the tumor region predicted by the model, and (c) the real tumor region as shown in the ground truth images.

- **Limited Validation in Real-World Settings:** While the approach may perform well in controlled research environments, it might not be extensively validated in diverse, real-world clinical settings. This gap in validation could limit its immediate applicability in everyday clinical practice.
- **Regulatory and Ethical Concerns:** The use of advanced AI models in healthcare raises regulatory and ethical issues, including patient privacy, data security, and the need for stringent validation before clinical deployment. Navigating these concerns is essential but can be challenging.

Distribution of rounded Ages in data

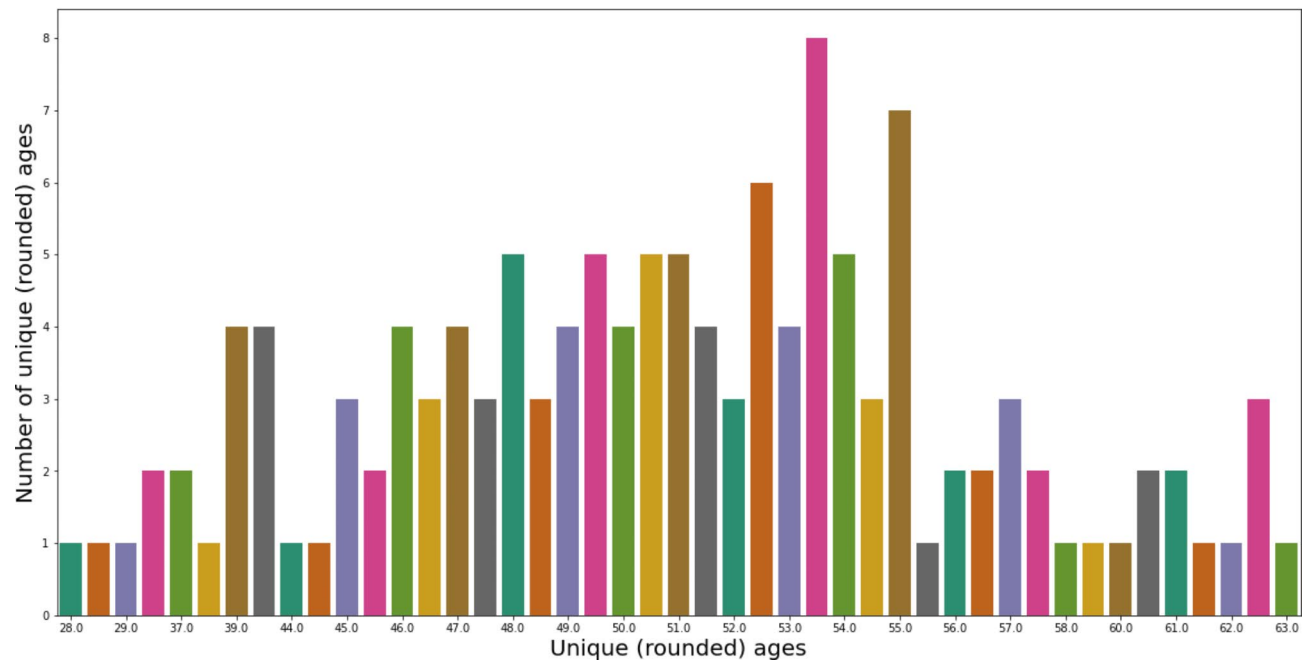


Fig. 16. Distribution of Rounded Ages in BRATS2020.

Distribution of rounded Survival_days in data

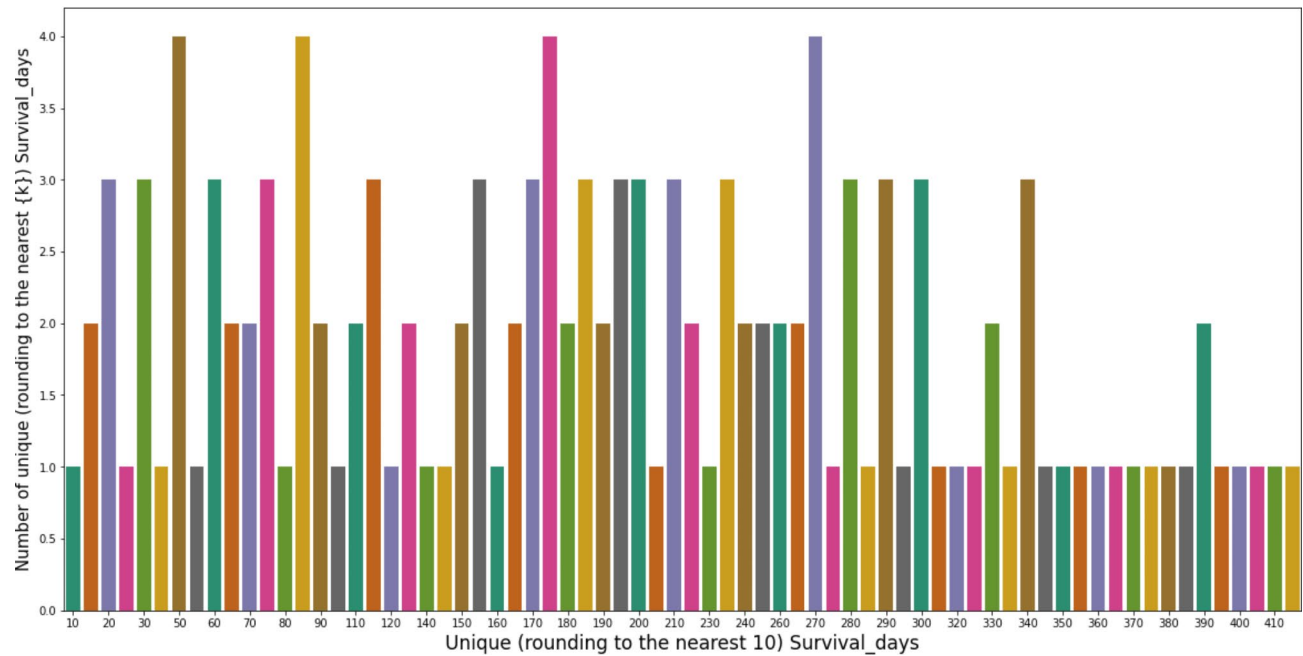


Fig. 17. Distribution of rounded Survival Days of patient as given in BRATS 2020.

	Loss	Accuracy	MeanIoU	Dice Coefficient	Precision
Train Result	0.097695	0.995166	0.616957	0.902311	0.995193
Validation Result	0.108875	0.994494	0.637059	0.891475	0.994538
Test Result	0.109715	0.994260	0.623013	0.889182	0.994220

Table 1. Evaluation report.

Reference	Model Used	Accuracy	DSC	Specificity	Sensitivity
¹	TPUAR-NET	-	0.89	0.99	-
⁶	LDI-Means + Mutual Information + Singular Value Decomposition With Dimensionality Reduction + SVM	0.9102	-	0.9426	0.93
¹³	VGG-16	-	0.8892	0.9948	0.9
¹⁴	U-Net Based CNN	-	0.878	0.993	0.87
²⁶	Deep Convolutional Neural Network	-	0.88	0.89	0.89
²⁷	3D-UNet	-	0.86	0.99	0.89
²⁸	Deep Convolutional Neural Network	-	0.87	0.94	0.82
³⁰	Fractional probabilistic Fuzzy C Means (Fr-pFCM) + Whale-Cat Swarm Optimization based Deep Belief Network (WCSO-DBN)	0.923	-	0.96	0.84
³⁶	Specital Fuzzy C Means	-	0.86	-	0.89
³⁴	Optimized Resnet50 with Gradcam	0.985	-	-	0.888
³⁹	Optimal DeepMRSeg + SPO + GAN + CAViaR-SPO.	0.917	-	0.925	0.8884
⁴¹	CNN	-	0.88	-	0.88
⁴⁸	Symmetric-Driven FCN	-	0.87	-	0.928
⁴⁹	Bayesian fuzzy clustering, Scattering transform (ST), Information-theoretic measures, Softmax Regression technique, DAE	0.985	-	0.995	0.95
⁵²	Handcrafted Convolutional Neural Network	0.95	0.91	0.96	-
⁵⁵	Cross-Level Connected U-Shaped Network (CLCU-Net	-	0.885	-	0.96
⁵⁹	FCNN + Conditional Random Fields	-	0.84	-	-
	Proposed Methodology	0.9951	0.9023	0.9980	0.9950

Table 2. Comparative analysis of the various BRATS dataset brain tumour segmentation techniques.

Implementing the MRI-based brain tumor feature extraction, segmentation, and survival days prediction approach using a Deep Learning Inspired Replicator Neural Network and Volumetric Convolution Network presents several challenges:

- **Data Heterogeneity:** MRI data can vary significantly across different machines, protocols, and institutions. This variability can affect model performance and generalization, necessitating robust preprocessing and normalization techniques.
- **Model Complexity and Computational Load:** The combined use of a Replicator Neural Network and Volumetric Convolution Network can be computationally intensive, especially when processing large, high-resolution 3D MRI scans. Ensuring efficient training and inference without sacrificing accuracy is a key challenge.
- **Limited Annotated Data:** Accurate tumor segmentation and survival prediction require well-annotated datasets, which can be scarce. The lack of sufficient labeled data for training can limit the model's ability to generalize, making techniques like data augmentation or synthetic data generation crucial.
- **Integration into Clinical Workflows:** Deploying this approach in real-world clinical settings involves integrating the model into existing medical imaging systems and ensuring it fits seamlessly into the clinician's workflow. This requires careful consideration of user interface design and real-time processing capabilities.
- **Interpretability and Trustworthiness:** Clinicians need to trust the model's predictions, particularly in critical decisions like survival prediction. Ensuring the model's outputs are interpretable and providing insights into how predictions are made will be vital for adoption in clinical practice.
- **Regulatory Compliance and Validation:** The model must meet stringent regulatory standards and undergo rigorous validation before being used in clinical environments. Ensuring compliance with healthcare regulations and demonstrating the model's safety and efficacy are significant hurdles.

Existing medical imaging systems face several practical and potential issues that impact their effectiveness and integration into clinical practice:

- **Scalability:** Many medical imaging systems struggle to scale with increasing data volumes and complexity. As imaging technology advances, systems must handle larger and higher-resolution datasets, which can strain existing infrastructure and require significant upgrades.

- **Integration Challenges:** Existing imaging systems often operate in isolation, making it difficult to integrate new technologies or updates. This can lead to fragmented workflows and inefficiencies, as new tools may not seamlessly connect with legacy systems, complicating data management and analysis.
- **Data Compatibility:** Different imaging modalities and systems may use various file formats and standards, creating issues with data compatibility. This lack of standardization can hinder the exchange of information between systems and reduce the ability to perform comprehensive analyses.
- **User Interface and Workflow:** Many existing systems have complex or outdated user interfaces that can be difficult to navigate. This can affect the convenience and efficiency of imaging procedures, leading to longer training times and potential errors in image interpretation.
- **Processing Speed and Storage:** High-resolution and 3D imaging generate large amounts of data, requiring significant processing power and storage capacity. Existing systems may struggle with processing speed and data storage, leading to delays and potential bottlenecks in clinical workflows.
- **Interoperability:** Ensuring that imaging systems work well with other healthcare technologies, such as electronic health records (EHRs) and diagnostic tools, is crucial for a cohesive patient care experience. Existing systems may have limited interoperability, making it challenging to integrate imaging data with other clinical information.

Integrating the proposed methodology into clinical workflows can enhance diagnostic accuracy and optimize patient care by streamlining and automating key processes. Seamless integration with existing medical imaging systems and electronic health records ensures compatibility and reduces disruptions. The methodology's advanced algorithms can improve tumor identification and localization, leading to more precise diagnoses and better-targeted treatments. Automation of routine tasks, such as image preprocessing and analysis, reduces workload and minimizes human error, allowing clinicians to focus on interpreting results. Real-time analysis capabilities provide immediate feedback during imaging procedures, facilitating quicker adjustments and more informed decisions. Enhanced data management and visualization tools offer clearer insights and comprehensive information for clinicians. Effective training and support for healthcare professionals ensure successful adoption and use of the new methodology. Additionally, quality control mechanisms and ongoing feedback help refine the methodology, maintaining high standards of accuracy and reliability. This integration ultimately improves diagnostic processes and patient care, contributing to better clinical outcomes.

Conclusion

This study involved using magnetic resonance imaging (MRI) of the brain to distinguish between normal brain tissue and tumor tissue, specifically gliomas. It is important to accurately identify and locate brain tumors to properly diagnose, treat, and estimate the patient's overall survival rate. To achieve this, the researchers employed a deep learning approach using a combination of MRI scans. They used a 2D Volumetric Convolutional Network architecture with a majority rule to ensure reliable tumor segmentation and improve performance. The researchers also extracted radiomic features from the segmented tumor regions and used a Deep Learning Inspired 3D Replicator neural network to identify the most effective features for predicting survival rates. In comparison to manual identification by clinical specialists, the findings demonstrated that the model accurately segregated brain tumours and forecasted the fate of enhancing and genuine enhancing tumours. The proposed methodology provides an accurate and speedy detection of brain tumors and precise location of the tumour. The study's findings are crucial for clinical practice, offering insights that can enhance patient care and outcomes. By integrating these results, clinicians can improve treatment effectiveness and tailor interventions, leading to better patient management and health outcomes. Accurate identification and localization of brain tumors are critical for improving diagnosis and treatment planning. Precise detection ensures that tumors are correctly identified, enabling targeted treatment strategies. Accurate localization helps in planning surgical interventions and other therapies, minimizing damage to healthy brain tissue. Overall, these advancements lead to more effective treatment, better outcomes, and improved patient care. Future research on this approach could focus on integrating multimodal data, such as genetics and other imaging types, to improve prediction accuracy. Developing personalized treatment models and optimizing for real-time processing would enhance clinical utility. Transfer learning could be explored to improve generalizability across diverse populations and MRI settings.

Data availability

The corresponding author will give the information used to back up the findings of this investigation upon request.

Received: 21 April 2024; Accepted: 23 December 2024

Published online: 09 January 2025

References

1. Abd-Ellah, M. K., Khalaf, A. A. M., Awad, A. I. & Hamed, H. F. A. TPUAR-Net: two parallel U-Net with asymmetric residual-based deep convolutional neural network for Brain Tumor Segmentation. In (eds Karray, F., Campilho, A. & Yu, A.) *Image Analysis and Recognition* (106–116). Springer International Publishing. (2019).
2. Abdel-Maksoud, E., Elmogy, M. & Al-Awadi, R. Brain tumor segmentation based on a hybrid clustering technique. *Egypt. Inf. J.* **16** (1), 71–81. <https://doi.org/10.1016/j.eij.2015.01.003> (2015).
3. Abdollahi, A., Pradhan, B. & Alamri, A. VNet: an end-to-end fully convolutional neural network for road extraction from High-Resolution Remote Sensing Data. *IEEE Access*. **8**, 179424–179436. <https://doi.org/10.1109/access.2020.3026658> (2020).
4. AboElenein, N. M., Piao, S., Noor, A. & Ahmed, P. N. MIRAU-Net: an improved neural network based on U-Net for gliomas segmentation. *Sig. Process. Image Commun.* **101**, 116553. <https://doi.org/10.1016/j.image.2021.116553> (2022).

5. Ain, Q., Jaffar, M. A. & Choi, T. S. Fuzzy anisotropic diffusion-based segmentation and texture based ensemble classification of brain tumor. *Appl. Soft Comput.* **21**, 330–340. <https://doi.org/10.1016/j.asoc.2014.03.019> (2014).
6. Al-Saffar, Z. A. & Yildirim, T. A hybrid approach based on multiple eigenvalues selection (MES) for the automated grading of a brain tumor using MRI. *Comput. Methods Programs Biomed.* **201**, 105945. <https://doi.org/10.1016/j.cmpb.2021.105945> (2021).
7. American Brain Tumor Association. <http://www.abta.org>
8. Amin, J. et al. Brain tumor detection by using stacked autoencoders in Deep Learning. *J. Med. Syst.* **44** (2), 32. <https://doi.org/10.1007/s10916-019-1483-2> (2019).
9. Ayadi, W., Elhamzi, W., Charfi, I. & Atri, M. A hybrid feature extraction approach for brain MRI classification based on bag-of-words. *Biomed. Signal Process. Control.* **48**, 144–152. <https://doi.org/10.1016/j.bspc.2018.10.010> (2019).
10. Bahadure, N. B., Ray, A. K. & Thethi, H. P. Image Analysis for MRI Based Brain Tumor Detection and Feature Extraction Using Biologically Inspired BWT and SVM. *International Journal of Biomedical Imaging*, 2017, 9749108. (2017). <https://doi.org/10.1155/2017/9749108>
11. Bashir-Gonbadi, F. & Khotanlou, H. Brain tumor classification using deep convolutional autoencoder-based neural network: multi-task approach. *Multimedia Tools Appl.* **80** (13), 19909–19929. <https://doi.org/10.1007/s11042-021-10637-1> (2021).
12. Caban, J. J., Yao, J. & Mollura, D. J. Enhancing image analytic tools by fusing quantitative physiological values with image features. *J. Digit. Imaging.* **25** (4), 550–557. <https://doi.org/10.1007/s10278-011-9449-z> (2012).
13. Cabezas, M., Valverde, S., González-Villà, S., Clérigues, A., Salem, M., Kushibar, K., ... Lladó, X. 2018. Survival prediction using ensemble tumor segmentation and transfer learning. arXiv preprint arXiv:1810.04274.
14. Caver, E., Liu, C., Zong, W., Dai, Z. & Wen, N. Automatic Brain Tumor Segmentation Using a U-net Neural Network. Pre-Conference Proceedings of the 7th MICCAI BraTS Challenge; 63. (2018).
15. Chaddad, A. Automated Feature Extraction in Brain Tumor by Magnetic Resonance Imaging Using Gaussian Mixture Models. *International Journal of Biomedical Imaging*, 2015, 868031. (2015). <https://doi.org/10.1155/2015/868031>
16. Chawla, R. et al. Brain tumor recognition using an integrated bat algorithm with a convolutional neural network approach. *Measurement: Sens.* **24**, 100426. <https://doi.org/10.1016/j.measen.2022.100426> (2022).
17. Chen, S. & Guo, W. Auto-Encoders in Deep Learning—A Review with New Perspectives. *Mathematics*, **11**(8), 1777. MDPI AG. (2023). Retrieved from <https://doi.org/10.3390/math11081777>
18. Cui, W., Wang, Y., Fan, Y., Feng, Y. & Lei, T. Localized FCM clustering with spatial information for Medical Image Segmentation and Bias Field Estimation. *Int. J. Biomed. Imaging*. **2013** (930301). <https://doi.org/10.1155/2013/930301> (2013).
19. Damodaran, S. & Raghavan, D. Combining tissue segmentation and neural network for brain tumor detection. *Int. Arab. J. Inform. Technol.* **12**, 42–52 (2015).
20. Deepak, S. & Ameer, P. M. Retrieval of brain MRI with tumor using contrastive loss based similarity on GoogLeNet encodings. *Comput. Biol. Med.* **125**, 103993. <https://doi.org/10.1016/j.comphbiomed.2020.103993> (2020).
21. Demirhan, A., Toru, M. & Guler, I. Segmentation of tumor and edema along with healthy tissues of brain using wavelets and neural networks. *IEEE J. Biomedical Health Inf.* **19** (4), 1451–1458. <https://doi.org/10.1109/JBHI.2014.2360515> (2015).
22. Gull, S., Akbar, S., Hassan, S. A., Rehman, A. & Sadad, T. Automated brain tumor segmentation and classification through MRI images. In (eds Liatsis, P., Hussain, A., Mostafa, S. A. & Al-Jumeily, D.) Emerging Technology Trends in Internet of Things and Computing (182–194). Springer International Publishing. (2022).
23. Guo, L. et al. Tumor detection in MR images using one-class Immune Feature Weighted SVMs. *IEEE Trans. Magn.* **47** (10), 3849–3852. <https://doi.org/10.1109/TMAG.2011.2158520> (2011).
24. Gupta, N., Bhatele, P. & Khanna, P. Glioma detection on brain MRIs using texture and morphological features with ensemble learning. *Biomed. Signal Process. Control.* **47**, 115–125. <https://doi.org/10.1016/j.bspc.2018.06.003> (2019).
25. Habib, H., Amin, R., Ahmed, B. & Hannan, A. Hybrid algorithms for brain tumor segmentation, classification and feature extraction. *J. Ambient Intell. Humaniz. Comput.* **13** (5), 2763–2784. <https://doi.org/10.1007/s12652-021-03544-8> (2022).
26. Havaei, M. et al. Brain tumor segmentation with deep neural networks. *Med. Image. Anal.* **35**, 18–31. <https://doi.org/10.1016/j.media.2016.05.004> (2017).
27. Hu, X. & Piraud, M. Multi-level Activation for Segmentation of Hierarchically-nested Classes on 3D-UNet. Pre-Conference Proceedings of the 7th MICCAI BraTS Challenge; 188. (2018).
28. Hussain, S., Anwar, S. M. & Majid, M. Segmentation of glioma tumors in brain using deep convolutional neural network. *Neurocomputing* **282**, 248–261. <https://doi.org/10.1016/j.neucom.2017.12.032> (2018).
29. Jemimma, T. A. & Raj, Y. J. V. Significant LOOP with clustering approach and optimization enabled deep learning classifier for the brain tumor segmentation and classification. *Multimedia Tools Appl.* **81** (2), 2365–2391. <https://doi.org/10.1007/s11042-021-1159-1-8> (2022).
30. Jemimma, T. A. & Vetharaj, Y. J. Fractional probabilistic fuzzy clustering and optimization based brain tumor segmentation and classification. *Multimedia Tools Appl.* **81** (13), 17889–17918. <https://doi.org/10.1007/s11042-022-11969-2> (2022).
31. Kapila, D. & Bhagat, N. Efficient feature selection technique for brain tumor classification utilizing hybrid fruit fly based abc and ann algorithm. *Materials Today: Proceedings*, 51, 12–20. (2022). <https://doi.org/10.1016/j.matpr.2021.04.089>
32. Kay, S. et al. Integrating Autoencoder and Heteroscedastic Noise Neural Networks for the Batch Process Soft-Sensor Design. *Ind. Eng. Chem. Res.*, **61**(36), 13559–13569. <https://doi.org/10.1021/acs.iecr.2c01789> (2022).
33. Kong, Y., Deng, Y. & Dai, Q. Discriminative clustering and feature selection for Brain MRI Segmentation. *IEEE. Signal. Process. Lett.* **22** (5), 573–577. <https://doi.org/10.1109/LSP.2014.2364612> (2015).
34. Kumar, M. M. R. M. T., Guluwadi, V. & S Enhancing brain tumor detection in MRI images through explainable AI using Grad-CAM with Resnet 50. *BMC Med. Imaging.* **24** <https://doi.org/10.1186/s12880-024-01292-7> (2024).
35. Kumar, P. & Vijayakumar, B. Brain Tumour Mr Image Segmentation and classification using by PCA and RBF Kernel based support Vector Machine. *Middle-East J. Sci. Res.* **23** (9), 2106–2116. <https://doi.org/10.5829/idosi.mejr.2015.23.09.22458> (2015).
36. Li, Q. et al. Glioma segmentation with a unified algorithm in Multimodal MRI images. *IEEE Access*, **6**, 9543–9553. <https://doi.org/10.1109/ACCESS.2018.2807698> (2018).
37. Louis, D. N. et al. The 2016 World Health Organization Classification of Tumors of the Central Nervous System: a summary. *Acta Neuropathol.* **131** (6), 803–820. <https://doi.org/10.1007/s00401-016-1545-1> (2016).
38. Maji, D., Sigedar, P. & Singh, M. Attention Res-UNet with guided decoder for semantic segmentation of brain tumors. *Biomed. Signal Process. Control.* **71**, 103077. <https://doi.org/10.1016/j.bspc.2021.103077> (2022).
39. Neelima, G., Chigurukota, D. R., Maram, B. & Girirajan, B. Optimal DeepMRSeg based tumor segmentation with GAN for brain tumor classification. *Biomed. Signal Process. Control.* **74**, 103537. <https://doi.org/10.1016/j.bspc.2022.103537> (2022).
40. Osborn, A. G., Louis, D. N., Poussaint, T. Y., Linscott, L. L. & Salzman, K. L. The 2021 World Health Organization Classification of Tumors of the Central Nervous System: what neuroradiologists need to know. *Am. J. Neuroradiol.* <https://doi.org/10.3174/ajnr.A7462> (2022).
41. Pereira, S., Pinto, A., Alves, V. & Silva, C. A. Brain tumor segmentation using Convolutional neural networks in MRI images. *IEEE Trans. Med. Imaging.* **35** (5), 1240–1251. <https://doi.org/10.1109/TMI.2016.2538465> (2016).
42. Rai, H. M., Chatterjee, K. & Dashkevich, S. Automatic and accurate abnormality detection from brain MR images using a novel hybrid UnetResNext-50 deep CNN model. *Biomed. Signal Process. Control.* **66**, 102477. <https://doi.org/10.1016/j.bspc.2021.102477> (2021).

43. Rastogi, D., Johri, P. & Tiwari, V. Brain tumor detection and localization: an inception V3 - based classification followed by RESUNET-Based Segmentation Approach. *Int. J. Math. Eng. Manage. Sci.* **8**, 336–352. <https://doi.org/10.33889/ijmems.2023.8.2.020> (2023b).
44. Sachdeva, J., Kumar, V., Gupta, I., Khandelwal, N. & Ahuja, C. K. Segmentation, feature extraction, and Multiclass Brain Tumor classification. *J. Digit. Imaging.* **26** (6), 1141–1150. <https://doi.org/10.1007/s10278-013-9600-0> (2013).
45. Sachdeva, J., Kumar, V., Gupta, I., Khandelwal, N. & Ahuja, C. K. A package-SFERCB-Segmentation, feature extraction, reduction and classification analysis by both SVM and ANN for brain tumors. *Appl. Soft Comput.* **47**, 151–167. <https://doi.org/10.1016/j.asoc.2016.05.020> (2016).
46. Salem, A. B. M. An Automatic Classification of Brain Tumors through MRI Using Support Vector Machine. (2016).
47. Sharma, N. et al. Segmentation and classification of medical images using texture-primitive features: application of BAM-type artificial neural network. *J. Med. Phys.* **33** (3), 119–126. <https://doi.org/10.4103/0971-6203.42763> (2008).
48. Shen, H., Zhang, J. & Zheng, W. Efficient symmetry-driven fully convolutional network for multimodal brain tumor segmentation. *2017 IEEE Int. Conf. Image Process. (ICIP)*, 3864–3868. <https://doi.org/10.1109/ICIP2017.8297006> (2017).
49. Siva Raja, P. M. & rani, A. V. Brain tumor classification using a hybrid deep autoencoder with bayesian fuzzy clustering-based segmentation approach. *Biocybernetics Biomedical Eng.* **40** (1), 440–453. <https://doi.org/10.1016/j.bbce.2020.01.006> (2020).
50. Tong, J., Zhao, Y., Zhang, P., Chen, L. & Jiang, L. MRI brain tumor segmentation based on texture features and kernel sparse coding. *Biomed. Signal Process. Control.* **47**, 387–392. <https://doi.org/10.1016/j.bspc.2018.06.001> (2019).
51. Torheim, T. et al. Classification of dynamic contrast enhanced MR images of cervical cancers using texture analysis and support Vector machines. *IEEE Trans. Med. Imaging.* **33** (8), 1648–1656. <https://doi.org/10.1109/TMI.2014.2321024> (2014).
52. Ullah, F. et al. Brain tumor segmentation from MRI images using handcrafted convolutional neural network. *Diagnostics* **13**, 2650. <https://doi.org/10.3390/diagnostics13162650> (2023).
53. Varuna Shree, N. & Kumar, T. N. R. Identification and classification of brain tumor MRI images with feature extraction using DWT and probabilistic neural network. *Brain Inf.* **5** (1), 23–30. <https://doi.org/10.1007/s40708-017-0075-5> (2018).
54. Wang, G., Xu, J., Dong, Q. & Pan, Z. Active contour model coupling with higher order diffusion for medical image segmentation. *International Journal of Biomedical Imaging*, 2014, 237648. (2014). <https://doi.org/10.1155/2014/237648>
55. Wang, Y. L., Zhao, Z. J., Hu, S. Y. & Chang, F. L. CLCU-Net: cross-level connected U-shaped network with selective feature aggregation attention module for brain tumor segmentation. *Comput. Methods Programs Biomed.* **207**, 106154. <https://doi.org/10.1016/j.cmpb.2021.106154> (2021).
56. Yang, F., Thomas, M. A., Dehdashti, F. & Grigsby, P. W. Temporal analysis of intratumoral metabolic heterogeneity characterized by textural features in cervical cancer. *Eur. J. Nucl. Med. Mol. Imaging.* **40** (5), 716–727. <https://doi.org/10.1007/s00259-012-2332-4> (2013).
57. Yao, J., Chen, J. & Chow, C. Breast Tumor Analysis in dynamic contrast enhanced MRI using texture features and Wavelet Transform. *IEEE J. Selec. Topics Signal Process.* **3** (1), 94–100. <https://doi.org/10.1109/JSTSP.2008.2011110> (2009).
58. Zanaty, E. Determination of Gray Matter (GM) and White Matter (WM) volume in Brain magnetic resonance images (MRI). *Int. J. Comput. Appl.* **45**, 975–981 (2012).
59. Zhao, X. et al. A deep learning model integrating FCNNs and CRFs for brain tumor segmentation. *Med. Image. Anal.* **43**, 98–111. <https://doi.org/10.1016/j.media.2017.10.002> (2018).

Author contributions

D.R., M.D., S.K., J.K., P.F. and A.A.K. proposed the idea under the supervision of the P.J., and G.E. Moreover, D.R., J.K., M.D., S.K., P.F. and A.A.K. contributed in the experimental simulations and designing, while P.J., G.E. and A.A.K. worked on the mathematical modeling. Also, D.R., M.D., S.K., P.F. and A.A.K. wrote the manuscript under the fruitful suggestions of J.K., P.J., G.E. All authors have read and agreed to the published version of the manuscript.

Declarations

Competing interests

The authors declare no competing interests.

Additional information

Correspondence and requests for materials should be addressed to A.A.K. or J.K.

Reprints and permissions information is available at www.nature.com/reprints.

Publisher's note Springer Nature remains neutral with regard to jurisdictional claims in published maps and institutional affiliations.

Open Access This article is licensed under a Creative Commons Attribution-NonCommercial-NoDerivatives 4.0 International License, which permits any non-commercial use, sharing, distribution and reproduction in any medium or format, as long as you give appropriate credit to the original author(s) and the source, provide a link to the Creative Commons licence, and indicate if you modified the licensed material. You do not have permission under this licence to share adapted material derived from this article or parts of it. The images or other third party material in this article are included in the article's Creative Commons licence, unless indicated otherwise in a credit line to the material. If material is not included in the article's Creative Commons licence and your intended use is not permitted by statutory regulation or exceeds the permitted use, you will need to obtain permission directly from the copyright holder. To view a copy of this licence, visit <http://creativecommons.org/licenses/by-nc-nd/4.0/>.

© The Author(s) 2025